1

Nanomaterials

This chapter[1] is not an exhaustive review of nanomaterials. Its objective is to describe some of the carbon-based and inorganic nanomaterials, frequently used in the design of sensors. Some nanomaterials with opto-electronic properties that have not really been used in the design of sensors but also have specific properties that have led to their application in the biomedical field, in particular in biological imaging, will also be described.

1.1. Carbon nanomaterials

Fullerenes, carbon nanotubes (CNTs), nano-diamonds (NDs) and carbon quantum particles or carbon quantum dots (CQDs) were all discovered before the 2000s, followed by graphene in 2005. Due to their remarkable physicochemical properties, fullerenes, CNTs and graphene (G) have given rise to innumerable applications and their exploitation has remained continuous, but with a much quicker development of G compared to fullerenes and CNTs.

1.1.1. *Fullerenes*

In 1985, Kroto et al. (1985) discovered Buckminsterfullerene C_{60} (hereinafter referred to as fullerene C_{60}) and revealed its balloon-shaped structure, consisting of an assembly of sp^2 carbon atoms, organized in the form of pentagons (12) and hexagons (20). Fullerene chemistry then developed and gave rise to a multitude of applications, in fields as diverse as electronics, energy, biology and medicine. Along with C_{60} and C_{70}, the two most stable forms (Figure 1.1), new fullerenes were subsequently synthesized, with more carbon atoms.

1 This chapter is inspired by one of our previous books entitled *Nanotechnology and Nanomaterials for Energy* (Lacaze and Lacroix 2021). We have reused some illustrations.

1.1.1.1. *Electrophilic and antioxidant properties of fullerenes*

The electrophilic nature of fullerenes allows the formation of anions with six negative charges, corresponding to the acceptance of six electrons by lower unoccupied molecular orbitals (LUMOs). The progressive electrochemical reduction in six steps of C_{60} and C_{70} shows that the six reduction states of fullerene can be obtained with good stability (Xie et al. 1992) (Figure 1.1).

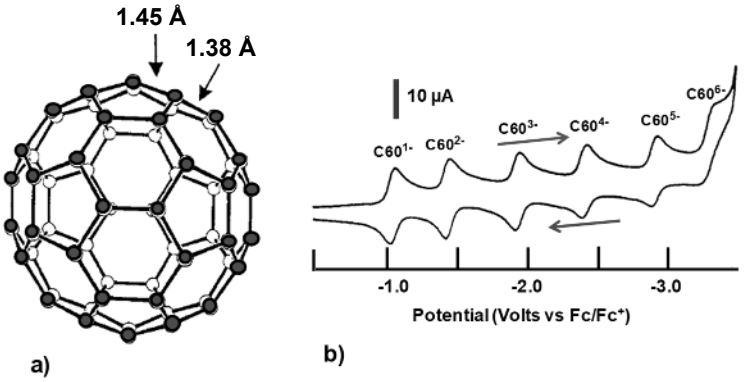

Figure 1.1. *(a) Image of fullerene C_{60}. Adapted from Balch et al. (1998). (b) Voltametric redox curves of C_{60} in solution in an acetonitrile/toluene mixture at low temperature (–10°C). Adapted from Xie et al. (1992). For a color version of this figure, see www.iste.co.uk/lacaze/nanotechnologies.zip*

COMMENT ON FIGURE 1.1.– *The red and white symbols (a) represent the C atoms in front and behind the projection plane. The reduction curve obtained by a potential sweep from –0.5 to –3.5 V (blue arrow) clearly shows the six reduction peaks, each corresponding to a gain of one electron. The reverse oxidation curve from –3.5 to –0.5 V (red arrow) shows six oxidation peaks, corresponding to the six intermediate and successive anionic states, thus proving the stability and reversibility of these six redox states. Scan rate: 100 mV/s.*

This electronic affinity has been exploited in the fields of medicine and biology. C_{60} and its derivatives, functionalized by various hydrophilic groups, have been used in the fight against cancer and AIDS (antiretroviral therapy against HIV-1). Functionalized by carbohydrate chains, they have also proven to be good antibacterial agents. Their high affinity for radicals, a property resulting from radical addition to the many fullerene double bonds, means that they are considered as "radical sponges". They are powerful antioxidants, used in biology to neutralize radical oxygen species (ROS), such as the superoxide ion $O_2^{-\bullet}$, hydroxyls $HO^{\bullet}$ or hydrogen peroxide H_2O_2, particularly impressive regarding DNA and certain

proteins. All these properties used for medical purposes have been described in review articles (Bakry et al. 2007; Lalwani and Sitharaman 2013; Acquah et al. 2017; Castro et al. 2017).

1.1.1.2. *Chemical reactivity and exofunctionalization*

Given their cage-shaped carbon structure, involving only covalent bonds between sp^2 carbons, fullerenes are naturally hydrophobic and therefore insoluble in aqueous environments. Their use for biological purposes requires transformations to make them hydrophilic, which is achieved by the grafting of hydroxyl groups (COOH or OH), corresponding to exofunctionalization reactions, typically carried out with C_{60}, and some commercially produced fullerenes (C_{70}, C_{80}, etc.), however at high prices, because of the difficulties in producing them in large quantities (Taylor and Walton 1993; Georgakylas et al. 2015).

Among all the products derived from fullerenes, fullerenols and carboxyfullerenes, obtained by grafting hydroxyl or carboxylic groups onto the surface of fullerenes, have the advantage over simple fullerenes in that they are soluble in aqueous and biological media. This is the case of hexacarboxylated fullerenes (carboxyfullerenes), which are fullerenes with three pairs of carboxylic acids, composed of a mixture of two stereoisomers, C3-C_{60} and D3-C_{60} (Figure 1.2)[2].

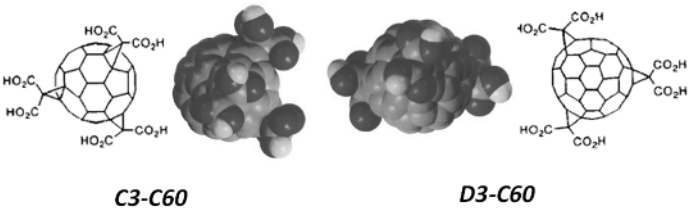

Figure 1.2. *Structure of the two stereoisomeric carboxyfullerenes C3-C_{60} and D3-C_{60} as per Dugan et al. (1997). For a color version of this figure, see www.iste.co.uk/lacaze/nanotechnologies.zip*

Like simple fullerenes, but with the added advantage of solubility in aqueous media, they have strong antioxidant properties, including the ability to destroy the peroxide ion $O_2^{\bullet -}$, a toxic by-product of cell metabolism. This property makes them very good neuroprotective agents, and research in this area is still ongoing (Dugan et al. 1997; Ali et al. 2004; Gharbi et al. 2005; Ye et al. 2015).

2 Both isomers, C3-C_{60} and D3-C_{60}, obtained by reacting ethyl 2-bromomalonate with C_{60} in the presence of NaH, belong to different symmetry groups (C3 and D3).

1.1.1.3. *Endometallofullerenes (EMFs)*

The presence of a cavity allows the encapsulation of chemical species, which is of interest for the design of various markers, used for example in medical imaging. As early as 1985, Smalley et al. identified with mass spectrometry the first fullerene with 60 carbon atoms containing a lanthanum atom (Heath et al. 1985). A few years later, they isolated several metallofullerenes with 60, 70, 74 and 82 carbon atoms, the latter $La@C_{82}$[3] being the only one that is stable in contact with air (Chai et al. 1991).

What is remarkable is that for all these new compounds there is no metal release when the compound is placed in a biological medium, which is a considerable improvement compared to metal chelates. This stability is likely due to the transfer of electrons between the La atom and the fullerene, which leads to the ion pair $La^{3+}@C_{82}^{3-}$, and to the fact that fullerene meshes are small enough that they prevent diffusion of the ion La^{3+} outward.

This discovery, which opened promising prospects in the medical field for diagnostic and therapeutic applications, triggered significant research into the synthesis of new EMFs, with some having applications in cancer therapy. Thus, gadolinium fullerenol $Gd@C_{82}(OH)_{22}$, initially used as a contrast agent in nuclear magnetic resonance imaging (MRI), also turned out to have a strong anti-cancer activity, different from that of simple fullerene, with low cytotoxicity (Kang et al. 2014)[4].

1.1.2. *Carbon nanodiamonds (NDs)*

Although known since the 1960s[5], they only began to be exploited at the end of the 1990s when they were produced by detonation of a mixture of explosive

3 The notation $La@C_{60}$ indicates that the lanthanum atom is inside the cage formed by the fullerene.

4 The gadolinium ion (Gd^{3+}), used as a contrast agent in NMR imaging, has the disadvantage of being very toxic. This toxicity can be greatly reduced when Gd is encapsulated in a hydrophilic fullerene, soluble in biological media, after exo-functionalization by OH or COOH groups of the fullerene molecule.

5 First discovered by Danilenko et al. in 1963 and overlooked by the scientific community, they were synthesized a second time in 1982 by another Russian team, during research into the synthesis of diamonds using the detonation technique in a pressurized chamber (Danilenko 2004). Obtained in the form of carbonaceous soot and considered uninteresting by-products, they only really began to interest scientists when they realized their functionalization capacity and areas of exploitation in the biomedical field.

products (trinitrotoluene [TNT] and trinitrobenzene [TNB]) (Greiner et al. 1988). These nanomaterials are now produced commercially. They are used for medical, diagnostic and therapeutic purposes, or to improve the mechanical properties of plastics.

From a mechanical point of view, NDs inherited properties from pure diamonds. They are characterized by their very high hardness and a very high Young's elasticity modulus, making them ideal for use in polishing hard surfaces (ceramics). Their very high chemical stability also allows them to be used in very aggressive environments. Two other particularly interesting properties are their fluorescence and biocompatibility, which make them suitable for biomedical applications (diagnosis and treatment) due to their easy surface functionalization.

Fluorescent nanodiamonds (FNDs) are a new family of nanomaterials, with sizes between 35 and 100 nm (Hsiao et al. 2016) and characterized by the presence of a structural defect inside the crystal (Figure 1.3(a)). This defect, called the nitrogen-vacancy (NV) defect, corresponds to a coupling between a vacancy (absence of a carbon atom in the lattice) and a nitrogen atom, adjacent to the vacancy. It can be easily created by irradiation of NDs crystallites with a helium (He^+) or proton (H^+)[6] ion beam. The processed NDs (equivalent to n-doped NDs) emit stable red fluorescence when excited by a laser. The intensity of the fluorescence depends on the concentration of NVs, which itself is higher the higher the energy of the He^+ ion beam used for their manufacture (the concentration of NVs can vary between 10 and 30 ppm in relation to the number of carbon atoms; when unprocessed their concentration is less than 1 ppm)[7].

Their biocompatibility, high stability, absence of toxicity as well as their high fluorescence intensity in the red make them diagnostic tools of choice in biology rather than inorganic quantum dots (QDs), which are most often made up of toxic elements Cd, Se, Pb, etc. (Chambers et al. 2008).

6 The sub-micron diamond powders used to make FNDs are obtained at high temperature and high pressure and contain approximately 100 ppm of nitrogen atom impurities dispersed throughout the diamond structure. Under the effect of ion bombardment, vacancies (V) are produced, their migration and their proximity to nitrogen atoms (N) leads to the formation of NVs centers.

7 NVs centers can exist in two forms NV° and NV^-, with NV^- dominating. NV^- determines the magneto-optical properties due to its different spin numbers $m_s = 0$ and ± 1. NVs are characterized by a strong absorption band centered at 550 nm and an intense fluorescence band around 685 nm, with a high quantum yield (70%) (Schirhagl et al. 2014).

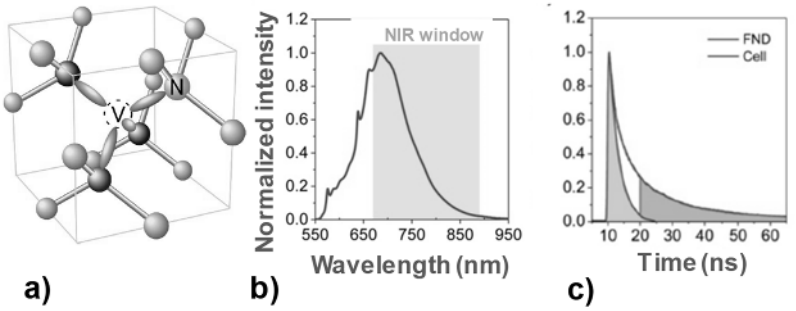

Figure 1.3. *Fluorescence of ND nanocrystals with NV defects. (a) Structure of an NV defect. (b) Fluorescence spectrum of FNDs (size 35 nm) obtained by laser excitation at 532 nm. (c) Differences between the fluorescence lifetimes of an FND (pink) and that of biological tissue (cell) due to the presence of endogenous fluorophores (green). According to Hsiao et al. (2016). For a color version of this figure, see www.iste.co.uk/lacaze/nanotechnologies.zip*

COMMENT ON FIGURE 1.3.– *An NV defect results from the proximity between a nitrogen atom (impurity due to the preparation of NDs) and a vacancy corresponding to the absence of a carbon atom. The ovals shown in purple (a) correspond to the dangling bonds of the carbon atoms neighboring the vacancy. The rectangle colored in pink (b) represents the spectral operating window for NDs, for which the autofluorescence of a biological tissue (green curve in c) is negligible. The fluorescence of the NDs can thus be detected by imposing a delay of 10 ns between the excitation and the detection of the emission (c).*

1.1.3. *Carbon quantum dots*

Less than 10 nm in size, they comprise a graphitic sp^2 carbon core, corresponding to fragments of graphene or graphene oxide (GO), linked together by sp^3 carbons. They contain significant amounts of oxygen on their surface, mainly as COOH, carbonyls and hydroxyl groups (Lim et al. 2015) (Figure 1.4).

Discovered by chance during the preparation and purification of CNTs (Xu et al. 2004), they quickly generated great interest because of their fluorescence properties, which make them potential biomedical imaging reagents. As with NDs, their non-toxicity is also an additional advantage, favoring their use in the medical field over inorganic QD semiconductors, which are often made with heavy metals.

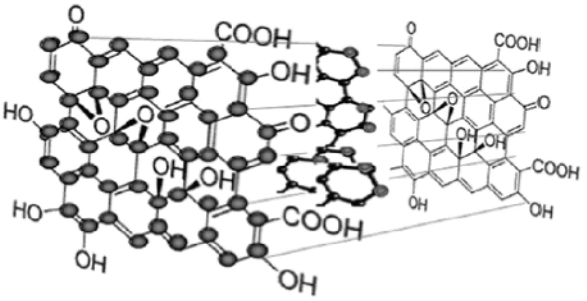

Figure 1.4. *Structure of carbon quantum dots (CQDs) showing the association between graphene oxide and graphene fragments. According to Lim et al. (2015) and Demchenko and Dekaliuk (2013)*

Unlike inorganic QDs, for which the absorption is determined by the band gap, CQDs are characterized by a very wide absorption band resulting from plasmonic absorption of the π[8] orbitals. This absorption band covers a large part of the UV-visible spectrum and extends into the near infrared spectrum, thus intercepting a large part of the solar spectrum (Fernando et al. 2015).

Two main emission mechanisms, not always easy to identify, are responsible for the fluorescence of CQDs. The first results from transitions between energy levels of sp^2 carbon bonded domains. The second is less obvious and it involves the surface defects present on the CQDs. A third type of mechanism, corresponding to up-conversion, has also been identified, where an emission is observed in the visible due to an excitation in the red (Figure 1.5).

The photoexcitation of CQDs is said to produce a separation of charges in the carbon cores. Their recombination with surface defects produces fluorescence, which also explains the great diversity of emissions, different from that observed with inorganic semiconductor QDs, characteristic of their band gaps.

One of the most striking characteristics of CQD fluorescence emission is the dependence of the emission spectrum on the excitation source. This has been attributed to different factors, such as the quantum size effect, the defects and surface states present in CQDs, the presence of fluorophores with different conjugation lengths, the radiative recombination of electron-holes due to sp^2 carbon clusters within a sp^3 carbon matrix, each of which are decisive and can contribute to fluorescence (Wang and Hu 2014).

8 Plasmonic absorption corresponds to a collective excitation of π electrons delocalized over several benzene cycles.

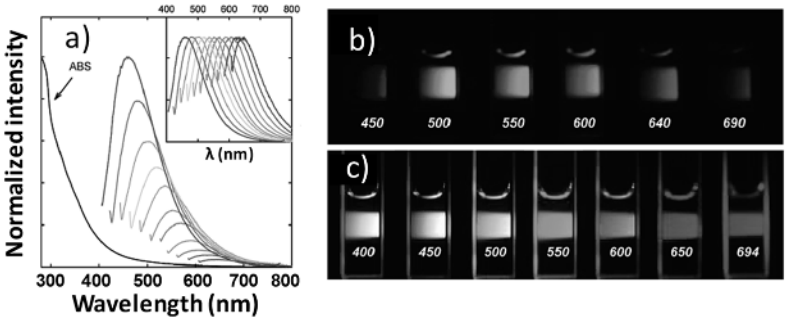

Figure 1.5. *Luminescence of an aqueous solution of CQDs produced by laser ablation of a graphite powder. (a) Absorption (ABS) and luminescence spectra obtained by excitation at different wavelengths (from 400 to 600 nm in 20 nm increments – from left to right). (b) Photographs of the luminescence of solutions of CQDs functionalized with polyethylene glycol (PEG) with a molar mass of 1,500 and comprising two amino groups at its chain ends –CH_2NH_2 (PEG_{1500N}). (c) The same solutions of CQDs are directly photographed after excitation at 400, 450 and 694 nm. According to Sun et al. (2006). For a color version of this figure, see www.iste.co.uk/lacaze/nanotechnologies.zip*

COMMENT ON FIGURE 1.5.– *CQDs (a) are functionalized by poly(propionylethyleneimine-co-ethyleneimine) (PPEI-EI), and the intensities are normalized to the quantum yields. Normalization is performed relative to peak intensity. The photographs in (b) correspond to an excitation at 400 nm of the CQDs and are obtained after passing the emitted light through color filters of 450, 500…690 nm.*

The fluorescence quantum yields of most CQDs are typically around 10%; in some cases, however, high yields of around 80% have been observed and seem to be linked to the presence of nitrogen resulting from the precursors used during pyrolysis (citric acid and ethylene diamine) (Zhu et al. 2013).

Finally, for certain CQD preparation conditions, multiphoton absorption was also observed, corresponding to the up-conversion of the emitted photons, which is an essential property for biomedical imaging, where excitation can be produced in the near-infrared spectrum (800–900 nm) with very high penetration of biological tissues (several mm). Such a property was discovered by Sun and colleagues (Cao et al. 2007), with CQDs of sizes of around 5 nm, passivated by a nitrogen-containing polymer (polypropionylimine-co-ethylenimine).

Given the ease of their production and the numerous functionalization possibilities of their surface, the production of various multifunctional probes can be considered. By combining, for example, magnetism and luminescence properties, MRI and fluorescence imaging can be performed simultaneously. Such a result has been demonstrated with the fixation of nuclear resonance contrast agents (gadolinium complexes) on fluorescent CQDs (Bourlinos et al. 2012).

Their solubility in an aqueous medium makes them diagnostic agents and very good vectors for transporting drugs to diseased biological cells. For instance, platinum salt-based anticancer drugs have been bound onto CQDs (Zheng et al. 2014a). Other applications have also been described (Wang and Hu 2014; Hu et al.2019a) and relate to optoelectronics (photovoltaics and electroluminescence), energy and its storage (supercapacitors and electrodes for lithium batteries) and analytical chemistry with the design of various sensors based on optoelectronic phenomena (Molaei 2020; Nazri 2021).

1.1.4. *Carbon nanotubes*

Iijima (1991) was the first to show the formation of multi-wall carbon nanotubes (MWCNTs) through the electrical discharge between carbon electrodes under a reduced argon-pressurized environment. He thus obtained a mixture of MWCNTs with diameters between 4 and 30 nm, approximately 1 μm long, made up of two to seven concentric tubes. Single-wall carbon nanotubes (SWCNTs) were obtained shortly after using cobalt-based catalysts (Bethune et al. 1993). These nanotubes have walls with a structure identical to that of graphene, which is made up of an assembly of sp^2-hybridized carbon atom monolayers, forming regular hexagons between them.

Since the first productions and characterizations of CNTs, numerous manufacturing and separation techniques have been introduced by several teams and are described in several articles (Grobert 2007; Hersam 2008; Komatsu and Wang 2010; Chen et al. 2014a). Essentially, the vaporization of carbon by laser ablation, the electrical discharge between graphite electrodes, catalytic chemical vapor decomposition (CCVD), the HiPco process (decomposition of CO under high pressure)[9] and the use of silica nanoparticles doped with Co (Co-MCM 41)[10] are the

9 The HiPco (high-pressure carbon monoxide) process was developed in the 1990s at Rice University. It makes it possible to obtain high purity SWCNTs by reacting carbon monoxide mixed with iron pentacarbonyl $Fe(CO)_5$ at high temperature (900–1,100°C) under a pressure of 30–50 atmospheres. The amount of CNTs produced using this process is around 450 mg per hour and provides a SWCNT mixture with 10 distinct chiralities (Bronikowski et al. 2001).

main CNT manufacturing methods. The choice of catalyst, as well as the carbon precursor fragmentation technique, is crucial. The CCVD technique is the most widespread as it is more likely to produce SWCNTs in large quantities, which is more favorable for production on a commercial scale (Figure 1.6).

The CVD technique typically involves introducing a gaseous carbon source (ethylene, acetylene, toluene, CO, etc.) mixed with a carrier gas (H_2, argon) into a reactor. The gas mixture, heated to a high temperature of at least 600°C corresponding to the decomposition of the carbon precursor, comes into contact with the catalyst (in the form of metal nanoparticles) on which the CNTs will develop.

The old electrochemical route is also the subject of research into the production of large quantities of carbon nanomaterials, such as graphene, carbon fibers, CDs and CNTs. The reduction of CO_2 in the form of molten carbonate is a solution that was recently developed by the Pint group to produce CNTs and has the merit of converting CO_2 into high added value products (Douglas and Pinta 2017).

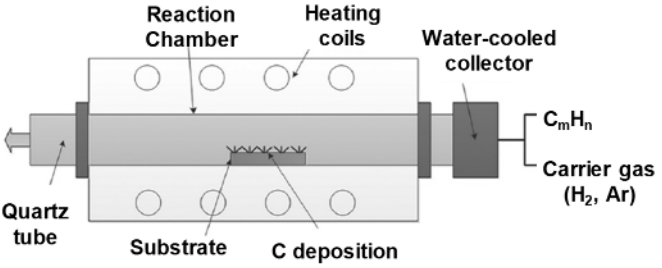

Figure 1.6. *Simplified schematic of the CVD device used to produce CNTs. Adapted from Gore and Sane (2011)*

Most manufacturing techniques produce CNT mixtures of multi-walled (MWCNTs) and single-walled nanotubes (SWCNTs) with different architectures, corresponding to distinct chiralities. The improvement of separation methods and the development of new catalysts, making it possible to increase the selectivity in the production of CNTs with a determined configuration or chirality, are important research topics.

10 MCM-41 is a particular zeolite whose pores can be adjusted between 2 and 10 nm. After depositing a thin layer of cobalt on its internal walls, the zeolite can be used as a nanoreactor to produce SWCNTs (Lim et al. 2003).

1.1.4.1. *Chirality of carbon nanotubes*

The formation of SWCNTs can be thought of as the result of rolling up a graphene fragment in a particular direction, defined by a C_h vector (Figure 1.7). This C_h vector, known as the chirality vector, is defined by the sum of vectors $\mathbf{a_1}$ and $\mathbf{a_2}$, forming a 60° angle between them. C_h is equal to n $\mathbf{a_1}$ + m $\mathbf{a_2}$, and the CNT with a chirality of (n, m) is thus obtained by rolling up the graphene fragment according to the direction of the vector C_h to connect the two ends of the vector. This makes the SWCNT circumference equal to the length of the C_h vector (Bachilo et al. 2002).

This chirality is particularly important because it determines the electrical properties of CNTs and, consequently, their use in fields such as nanoelectronics, photovoltaics, energy storage and sensors.

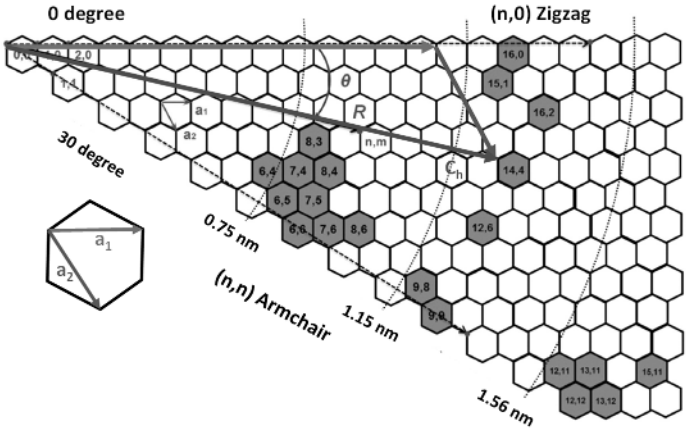

Figure 1.7. *Formation of an SWCNT defined by the rolling up of a graphene fragment along the direction of the chiral vector $C_h = na_1 + ma_2$. Adapted from Wang et al. (2015). For a color version of this figure, see www.iste.co.uk/lacaze/nanotechnologies.zip*

COMMENT ON FIGURE 1.7.– *The C_h vector (red arrow) equal to $14a_1 + 4a_2$ corresponds to the formation of an SWCNT with the chirality (14,4). An angle of Θ with respect to the a_1 vector axis defines an SWCNT (4,14) with R-type chirality (rectus), which has the same diameter as S-SWCNT (14,4) (sinister (S) chirality). The blue hexagons correspond to the most common CNT chiralities obtained synthetically with diameters between 0.7 and 2 nm.*

For SWCNTs with different chiralities (n,m), two limit forms, Armchair (n,n) and Zigzag (n,0) structures, are important and correspond to Θ angles of 0° and 30°, respectively (Figure 1.8). The Armchair (n,n) configuration has a metal-like conductivity; the Zigzag configuration (n,0) and SWCNTs of chiralities (n,m) also have metal-like conductivities but only when the difference between n and m is a multiple of 3 (Maultzsch et al. 2005) and are semiconductors when it is not the case. Band gaps are less than 1 eV and decrease as the CNT diameter increases (Odom et al. 1998).

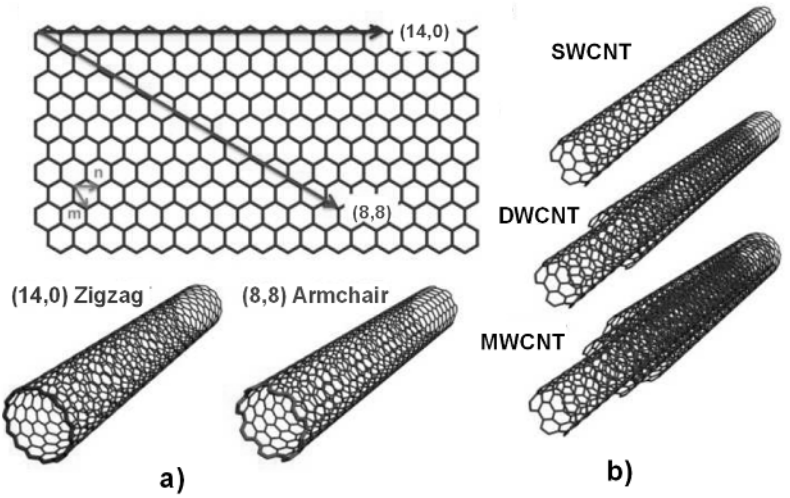

Figure 1.8. *Examples of CNTs with different configurations. (a) Examples of two SWCNTs (14,0) and (8,8) constructed from a graphene sheet, rolled according to the vectors (14,0) (red) and (8,8) (green) and corresponding to the two Zigzag and Armchair configurations. (b) Images of single-walled (SWCNT), double-walled (DWCNT) and multi-walled (MWCNT) CNTs. Adapted from Schnorr and Swager (2011). For a color version of this figure, see www.iste.co.uk/lacaze/nanotechnologies.zip*

Each configuration (n, m) corresponds to a distinct Raman spectrum and a particular CNT diameter, which allows them to be identified. The frequency of the Raman Radial Breathing Mode band (RBM), corresponding to the radial mode of vibration of the nanotube (ω_{RBM}), is linked to the diameter (d) by the relation:

$$\omega_{RBM} = A/d + B$$

A and B are experimentally determined constants (Bachilo et al. 2002; Maultzsch et al. 2005).

1.1.4.2. *Some properties and applications of CNTs*

The list of their properties is particularly long and well summarized in several review articles (De Volder et al. 2013; Yang et al. 2015; Ferrier 2021; Dai 2022).

CNTs are characterized by their high conductivity due to their metallic character. Wei et al. (2001) showed that MWCNTs could withstand current densities greater than 10^9 A/cm^2 over 2-week periods at temperatures between 200 and 250°C without observing any CNT degradation or variation in conductivity. CNT semiconductors are also characterized by extremely high electron and hole mobility properties, far beyond silicon, reaching up to 79,000 cm^2 V^{-1} s^{-1} (Dürkop et al. 2004). The band gap widths are inversely proportional to the CNT diameter and are approximately 1 eV for diameters of 1 nm, a value comparable to that of silicon (Kataura et al. 1999).

The thermal conductivity in the axial direction of a CNT is very high (3,500 Wm^{-1} K^{-1} for a SWCNT 2.6 μm in length and 1.7 nm in diameter, while for copper, a very good thermal conductor, it is only 385 Wm^{-1} K^{-1}; Pop et al. 2006). On the other hand, the thermal conductivity in a radial direction is very low at only 1.52 Wm^{-1} K^{-1}, almost a thermal insulator in this direction. This difference between the two orientations explains that for films made up of CNT assemblies arranged disorderly, the thermal conductivity is only 1,500 Wm^{-1} K^{-1} (Koziol et al. 2017). Note that, under a vacuum, these CNTs resist up to temperatures of 2,800°C and 750°C under an air atmosphere.

Ideal CNT structures lead to exceptional mechanical characteristics, with a tensile strength of 100 GPa (10^{11} Pascal), Young's modulus of 1 TPa (10^{12} Pascal), and an elongation at break of 18%. Such values were obtained with CNTs that were several centimeter long and defect free. The use of CNTs as polymer reinforcement fibers with the production of CNT/polymer composite materials is a key application area that has been the subject of numerous studies (Sun et al. 2013; Chen and Yan 2017a).

Obtaining self-supported films of agglomerated CNTs, leading to a buckypaper structure, coupling very good mechanical and electrical properties, is a commercially available product with numerous potential applications. Note that 6 μm thick buckypaper sheets can be made simply by vacuum filtration of an MWCNT dispersion; the film obtained has an elastic modulus of 3 GPa and a conductivity of about 2×10^4 S/cm, a function of the deformation state, which makes it a possible sensor for detecting movements (Degraff et al. 2017).

CNTs are widely used in nanoelectronics, energy, mechanics, biomedicine and sensors. Their use in the production of biosensors has been the subject of recent

research (Ferrier 2021; Dai 2022). Their exceptional properties have made CNTs successful and have encouraged many companies to develop large-scale preparation techniques. Over a few years (between 2004 and 2011), global production of CNTs has increased from 200 kg to 4,500 tons per year, a 22,500-fold increase (De Volder et al. 2013), reaching around 20,000 tons in 2022[11]. The cost of SWCNTs, however, remains high: it depends on the packaging method and varies depending on the companies that manufacture them. In 2020, the lowest prices were between $80 and $100 per kg, and the price of industrial-grade MWCNTs varies between $200 and $400 per kg.

1.1.4.3. *Conclusion*

CNTs are a family of nanomaterials whose strategic importance has continued to grow. Due to their exceptional electrical and mechanical properties, they have given rise to many applications thanks to very broad commercialization. However, obtaining large quantities of highly pure CNTs with a specific chirality is still challenging.

1.1.5. *Graphene*

Geim et al. were the first to isolate a fragment of graphene by mechanically exfoliating a sheet of graphite. The prepared graphene film is extremely stable, and a range of electrical and mechanical measurements can easily be done[12]. Moreover, monolayer of graphene can be easily identified by Raman spectroscopy. A characteristic line (G) appears at 1,584 cm^{-1}, as well as another line (2D or D') close to 2,700 cm^{-1}, whose width increases as the number of graphene layers increases (Ferrari et al. 2006; Graf et al. 2007; Bonaccorso et al. 2010).

The physical, chemical and mechanical properties discovered for graphene were exceptional and it immediately became the "magic" material at beginning of the 21st century. Its unique electrical properties make it a material of choice for electronics and allowed considerable improvements in the performance of various devices used in the fields of electronics, optoelectronics, energy and biomedical analysis. Since the 2010s, graphene-based transistors have been manufactured. However, the fact

11 A 2021 Fortunes Business Insights report forecasts an increase in the global CNTs market from 5.32 to 10.52 billion USD between 2021 and 2028, representing a CAGR of 10.2% for this period (ID: 5685490).

12 The technique may seem simple but, in fact, the graphene sheet deposited on a Si substrate covered with a thin layer of SiO_2 only becomes visible if an optical contrast occurs between the silica and the graphene. This implies that the thickness of the silica layer must be comparable with that of the graphene sheet. Geim and Novoselov (Nobel Prize in Physics in 2010) recognized that it was a fortunate combination of circumstances that allowed them to highlight the graphene monolayer (Geim and Novoselov 2007).

that graphene is a zero-bandgap material does not allow it to be used as a field-effect transistor for digital logic operations (Schwierz 2010). A band gap opening is necessary: One solution is to use graphene ribbons for which 200–300 meV band gaps have been obtained. Moreover, the variations in conductivity caused by the surface adsorption of chemical compounds are significant and can be exploited to produce various sensors (Pumera 2011).

1.1.5.1. *Extreme electrical properties of exfoliated graphene*

Graphene, made up of an assembly of sp^2 carbons organized according to a perfect two-dimensional hexagonal lattice, is a material with a zero bandgap.

The conductivity of graphene and the mobility of electrical charges are extremely high and have been extensively described in numerous articles by Geim, Novoselov, and their colleagues (Novoselov et al. 2004, 2005b; Geim and Novoselov 2007). It can be doped with positive or negative charges by applying an electric field. In contrast, with other two-dimensional semiconductors, an electric field only modulates the electron density (Novoselov et al. 2005a) (Figure 1.9(a)).

In the case of graphene, the charge carriers no longer obey the laws of non-relativistic classical quantum mechanics deduced from the Schrödinger equation, but instead those of Dirac's relativistic physics, where low-energy electrons are assimilated to massless quasi-particles with 1/2 spin. Conical-shaped valence and conduction energy bands intersect at a single point with zero energy and zero charge in the k vector wave space associated with these particles (Dirac point or neutrality point). One of the paradoxes of the theory is the existence of a non-zero conductivity at this neutrality point, even though the corresponding charge density is zero.

Figure 1.9(b) shows the differences in conductivity of graphene and two-dimensional semiconductor materials such as $NbSe_2$ and MoS_2, each incorporated as a field-effect transistor channel. In the case of graphene, the conductivity variation curve is perfectly symmetrical with respect to the axis $V_g = 0$ V. On the contrary, for $NbSe_2$ and MoS_2, a monotonic variation in conductivity versus Vg is observed.

The very high mobility values of over 150,000 cm^2/Vs cited in the literature can only be obtained for extremely pure graphene and correspond to a ballistic type of charge transport mechanism, for which the mean free path is approximately a micron. With impure graphene, the mobilities are much lower (around 15,000 cm^2/Vs) and have a transport mechanism partially controlled by diffusion; the mean free path of the charges is also smaller and is only around 150 nm (Bolotin et al. 2008a)[13].

13 The mean free path of electrons, a function of the applied electric field, is for most conductive elements between a few nm and a few tens of nm. In the case of copper, it is around 40 nm (Gall 2016).

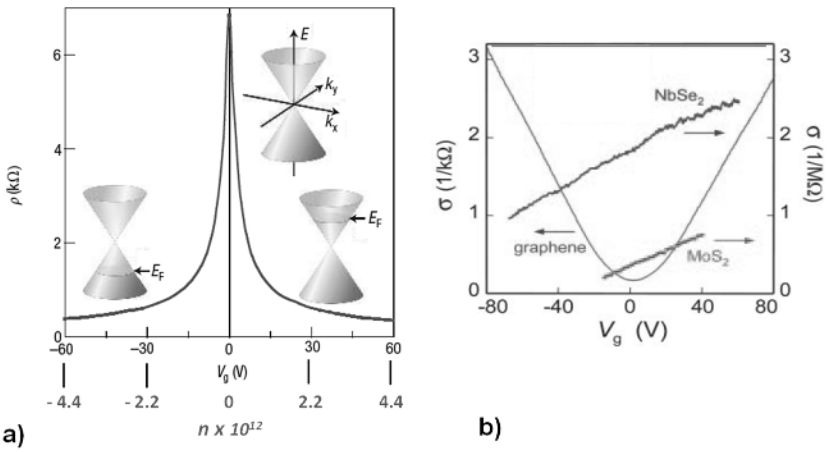

Figure 1.9. *Resistivity variations of graphene and 2D materials as a function of charge densities. (a) Resistivity ρ of a graphene sheet inserted as a channel in a field effect transistor subjected to a gate potential Vg. Adapted from Geim and Novoselov (2007). (b) Comparative conductivity curves of graphene and the 2D semiconductors MoS_2 and $NbSe_2$. According to Novoselov et al. (2005a, 2005b). For a color version of this figure, see www.iste.co.uk/lacaze/nanotechnologies.zip*

COMMENT ON FIGURE 1.9.– *The perfect symmetry of the curve $\rho_{xx} = f(V_g)$ relative to the axis $V_g = 0$ V corresponds to graphene completely free of impurities and is obtained at very low temperatures. Note that for a zero charge density, the resistivity of graphene maintains a finite value. The different conductivity regions are accompanied by diagrams of the energy bands and the Fermi level (E_F) corresponding to each polarization; negative and positive values of n correspond to the hole and electron densities. According to the device used, the electron or hole charge carrier densities vary linearly with the voltage according to the relationship $n = \alpha V_g$ with $\alpha = 7.2 \times 10^{10}$ $cm^{-2}V^{-1}$. Adapted from Geim and Novoselov (2007).*

1.1.5.2. *Graphene preparation techniques*

Several techniques for producing graphene for commercial purposes have been developed. This mainly involves chemical vapor deposition (CVD) and chemical and electrochemical exfoliation, with the latter having the advantage of producing graphene at a lower cost but of lower quality.

Of the many proposed techniques, growing graphene epitaxially on a SiC crystal under atmospheric argon pressure at high temperatures (1,650°C) avoids graphene transfer operations. This makes it possible to obtain a graphene film of the same size

as the crystal directly deposited on an insulating support, a necessary condition for producing field-effect transistors (Emtsev et al. 2009).

1.1.5.2.1. CVD on a solid catalyst

The first graphene deposits obtained by CVD were made on mono- or poly-crystalline nickel and copper substrates. The process uses a methane and hydrogen gas stream, heated to approximately 900–1,000°C, decomposing on contact with nickel or copper and releasing carbon atoms. These two processes have undergone numerous modifications. CVD formation conditions are like CNT formation conditions and only differ by the nature of the catalysts and higher temperatures. However, the deposits obtained on a copper substrate are of better quality than those obtained on nickel (Figure 1.10).

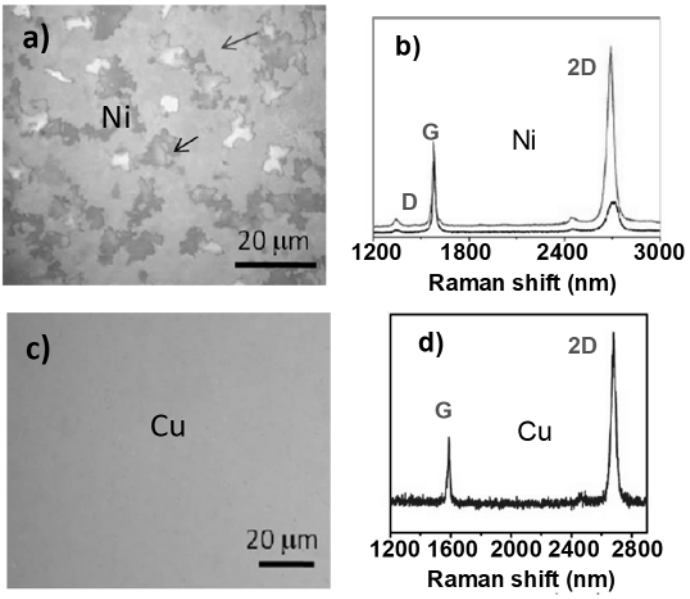

Figure 1.10 *Graphene deposits on Ni and Cu and transferred onto a Si/SiO_2 support. (a and c) Optical images of graphene fragments deposited on Ni and Cu, respectively. (b and d) Raman spectra of graphene for the graphene deposits on Ni and Cu. Adapted from Zhang et al. (2013a). For a color version of this figure, see www.iste.co.uk/lacaze/nanotechnologies.zip*

COMMENT ON FIGURE 1.10.– *Unlike the deposit synthesized on Ni, the graphene film obtained on Cu has great homogeneity. In the case of nickel (image a), the heterogeneity of the deposits (black and red arrows) is revealed by two distinct Raman spectra (b), one corresponding (in red) to a monolayer of graphene, with*

some defects (D band around 1,300 cm^{-1} non-zero), the other (in black) a multilayer deposit (characterized by a very low intensity of the 2D band). In the case of copper, the perfect homogeneity of the graphene film (image c) is confirmed by the unique presence of the two Raman bands 2D and G, with an I_{2D}/I_G intensity ratio equal to 2, characteristic of a monolayer of graphene (d).

The difference comes from the fact that in the case of copper, and although the experimental conditions (CH_4, H_2 and temperature) are comparable to those used with Ni (Li et al. 2009), the carbon atoms resulting from the dissociation of methane are poorly soluble in copper and adsorb directly to the surface of the metal to give graphene (Zhang et al 2013a). On the contrary, in the case of Ni, the carbon atoms coming from the dissociation of methane solubilize inside the nickel and, upon cooling, re-diffuse to the surface, then recombine to form a graphene film, which in the case of polycrystalline nickel, with many grain boundaries, gives poorer film homogeneity than with copper. This difference appears clearly in Figure 1.10, showing images of graphene films and their Raman spectra[14] for each metal.

1.1.5.2.2. CVD on a liquid catalyst

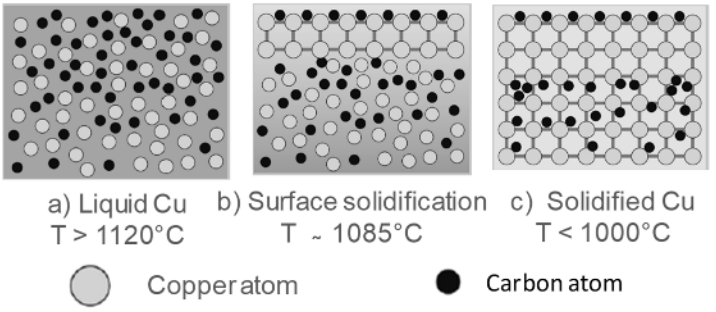

Figure 1.11. *Different stages of the catalytic process of forming a graphene monolayer. (a) Copper is in a liquid state with carbon atoms in solution; (b) initial cooling to 1,085°C produces surface crystallization of copper. (c) Further cooling blocks the graphene monolayer on the copper surface. Adapted from Zeng et al. (2014). For a color version of this figure, see www.iste.co.uk/lacaze/nanotechnologies.zip*

14 The different Raman bands of graphene films (G, 2D and D) make it possible to assess their thickness and the presence or absence of defects. A monolayer of graphene is characterized by a band intensity ratio I_{2D}/I_G close to 2, just as the thickness (evaluated by the number n of layers) can be measured from the position of the band G, which verifies the wave number relationship $\omega_G = 1581.6 + 11/(1 + n^{1.6})$ cm^{-1}. D Band only appears when graphene has defects and is located around 1300 cm^{-1}; 2D band, sometimes considered as a harmonic of the D band is very intense for a graphene monolayer and is located at 2750 cm^{-1}. It decreases in intensity and widens as the number of graphene layers increases (Wall 2011).

COMMENT ON FIGURE 1.11.– *During the initial cooling (b), the crystallization of Cu on the surface prevents the C atoms within the liquid from diffusing toward the surface. Thus, it is possible to maintain an organized monolayer of carbon on the copper surface to form graphene*.

The use of liquid metal catalysts in CVD is a new trend in the manufacturing of 2D materials. Applied to graphene, this method might improve its quality. This technique, described in detail by Zeng et al. (2014), is comparable to CVD methods, but differs in the use of the catalyst in the liquid state. Subjected to slow cooling, leading to the phase change from a liquid state to a solid surface state, the carbon atoms coming from the dissociation of the carbon precursor (CH_4), initially dissolved in the molten metal core, stop diffusing toward the surface as soon as it solidifies. This surface solidification limits the concentration of surface carbon atoms, thus promoting the formation of graphene monolayers (Figure 1.11).

1.1.5.2.3. The CVD process adapted to large-scale production

Given the strategic importance of graphene, numerous improvements to the CVD preparation process have been proposed in recent years to produce graphene on a large scale and at the lowest cost. The CVD process is in fact the only one suitable for the mass production of graphene by allowing two successive operations to be carried out continuously and automatically: the synthesis of graphene and the transfer of graphene to a flexible support. Adapting the roll-to-roll (R2R) printing process to the production of graphene, in the form of 30 cm wide several meter long films, is one of the most impressive examples. Many industrial groups have invested in this applied research topic, and it has been the focus of numerous university-industry consortia[15]. Several variants of the CVD process applicable to R2R technology have been proposed in recent years and have been well described by Xin et al. (2018). Large graphene films, adhering to flexible transparent plastic supports, were produced by this technique.

Bae et al. (2010) were among the first, in collaboration with Samsung, to produce rolled hybrid graphene glued to plastic using the R2R technique, up to 1 m long. Later, Kobayashi et al. (2013) from Sony produced graphene films using the R2R technique with qualities comparable to ITO plates and lengths over 100 m. They used a copper ribbon heated by the Joule effect to around 1,000°C that passed slowly into a chamber where a gas mixture of methane and hydrogen circulated at reduced pressure. Accurately adjusting the gas flow and the rate of the copper ribbon is decisive for obtaining a good quality single-layer graphene film. After forming the graphene film, it is automatically transferred onto plastic support, and the copper

15 Europe has funded a consortium between universities and companies in the industry for the development of large-scale graphene production techniques.

automatically dissolved, producing graphene coils 100 m long and 20 cm wide, characterized by a square resistance between 150 and 250 Ω/□[16] and an optical transmission of around 85% (Kobayashi et al. 2013).

1.1.5.2.4. Chemical methods to produce reduced graphene oxide (rGO) from GO

The starting product is graphite oxide, a multi-layer precursor of GO with very low conductivity. A wide variety of graphite oxidation methods have been described, the most frequently used is the oxidation of graphite powder using potassium permanganate[17]. Exfoliation is then done using strong ultrasound agitation in a liquid medium (Eigler et al. 2013). This chemical reaction leads to significant degradation of the crystal lattice, following the breaking of C-C bonds, resulting from oxidation with CO_2 release (Eigler et al. 2013).

Once GO is obtained, in the form of a suspension in a water-alcohol mixture (0.1 mg/mL), the GO is dispersed onto a solid support, then reduced with a mixture of hydriodic acid (HI) and trifluoroacetic acid (CF_3CO_2H) as a vapor, which gives reduced graphene rGO, deposited in the form of flakes sized between 500 nm and 1 μm[18]. A statistical Raman analysis of these rGO flakes shows that after reduction, according to the full width at half maximum (FWHM) of the 2D Raman band at 2,700 cm^{-1}, they can be classed into three distinct fractions: rGO with few.

FWHM <50 cm^{-1}) and a high proportion of rGO with many structural defects (FWHM > 50 cm^{-1}).

Graphene obtained by the reduction of GO does not have the same high purity as graphene obtained by mechanical exfoliation or CVD. However, although its conduction properties are less good than those of previous graphene, it can be produced at a lower cost without the need for large investments in equipment. Its mechanical and conduction characteristics are sufficient for many applications.

---

16 This notation, specific to electronic engineers, corresponds to a "square resistance" ($R\square = \rho/e$, ρ being the resistivity, and e the thickness). For example, a material of width W = 2 mm and length L = 3 mm, with a "square resistance" of 500 Ω/□, (500 Ω per square) will have the resistance $R = (L/W) \times R\square = 750\ \Omega$.

17 Hummers' method involves gradually adding potassium permanganate to graphite powder suspended in a solution of silver nitrate and sulfuric acid. The reaction is exothermic and can become explosive if the temperature is not controlled (Hummers and Offeman 1958). Starting from 1 g of graphite powder, Eigler et al. obtained 500 mg of GO and 200 mg of graphene after chemical reduction.

18 Using a mixture of hydriodic acid ($I^- + H_3O^+$) and trifluoroacetic acid as a GO reducing agent is a non-toxic alternative to hydrazine.

1.1.5.3. *Some applications of graphene and its derivatives*

The properties of single-layer graphene are exceptional. In addition to its low surface mass of 0.77 mg/m^2, it is in fact characterized at the mechanical level by a tensile strength of 130 GPa and by an elasticity modulus (E) of 1,100 GPa, whereas for stainless steel, E is around 200 GPa and its tensile strength is 0.5 GPa; its electrical conductivity (10^8 S m^{-1}) is greater than that of copper (6×10^7 S m^{-1}) and it can withstand current densities between 10^{10} and 10^{11} A m^{-2} without degrading. Its thermal conductivity is also very high with a record value of 5,300 Wm^{-1} K^{-1} while that of copper is only 400 Wm^{-1} K^{-1}. These values are obviously only obtained for graphene free of defects and impurities. However, for large-scale applications, which require graphene to be produced in large quantities, the record characteristics indicated previously are not achieved, but these are not always necessary. Reevaluating the required graphene production conditions in terms of quality, uniformity and reliability is necessary for more competitive products and devices, in terms of cost and performance[19].

For many applications, such as electrode materials, solar energy conversion devices, or energy storage with different battery systems, multilayer graphene sheets of medium quality may be sufficient. This is also the case for producing fibers used as electrical cables.

1.1.5.3.1. Graphene oxide

GO, obtained by the oxidation of graphite, can be seen as a stack of graphene sheets, functionalized in their plane (phenolic and epoxy) and at their ends (carboxylic) by oxygenated groups. Ultrasonic agitation in an aqueous medium exfoliates the sheets and produces a colloidal suspension in water of GO nanosheets with a thickness of approximately 1 nm and lateral dimensions varying by a few nanometers to several hundred micrometers. The solution can be filtered very slowly through a porous disk, producing a thick compact film. The thickness of these films can vary from 1 to 30 μm. The resulting paper-like product has very good mechanical properties due to the strong interactions between the hydroxyl groups. For films a few micrometer thick, the elasticity modulus (E) is around 30 GPa (Dikin et al. 2007), while for buckypaper, resulting from the agglomeration of CNTs, it is only around 7 GPa.

19 Consulting the Manchester Graphene Engineering and Innovation Centre (GEIC) website, as well as that of the Graphene Council, created in 2013, devoted to the development and exploitation of graphene, gives an idea of the vast number of current and potential applications for graphene prepared in different ways. Refer to the interview of T. Barkan (Graphene council), “The future of graphene”, February 2019 (AZOnano): https://www.azonano.com/article.aspx?ArticleID=5135.

1.1.5.3.2. Graphene paper and fibers obtained from rGO sheets

By reducing a suspension of GO with hydrazine followed by vacuum filtration, Li and colleagues obtained films with a metallic appearance and controllable thickness (from a few tens of nanometers to several micrometers) (Chen et al. 2008) (Figure 1.12). These films, which look like sheets of paper, are like the type of graphene, rGO. Very mechanically resistant, rGO is also a material with good electrical conduction properties, differentiating it from insulating GO.

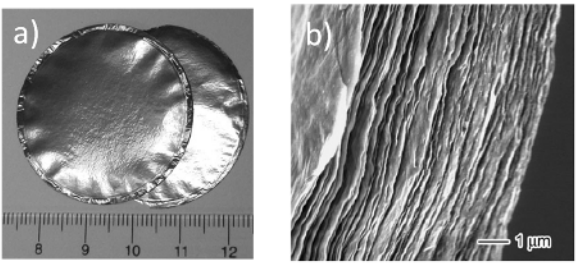

Figure 1.12. *Graphene paper (rGO) obtained after reducing graphene oxide (GO) sheets. (a) Photograph of two metallic-looking graphene sheets (front and back views). (b) Scanning electron microscopy (SEM) image of graphene paper showing the stacking of graphene sheets. According to Chen et al. (2008)*

Graphene paper's mechanical and electrical properties depend on the strength of the cohesion between the different layers. This cohesion is weakened by residual gases and liquids resulting from previous chemical processes. Located between the graphene sheets, these impurities are difficult to remove due to the impermeability of the sheets. An American team proposed solving this problem by intentionally creating holes on the surface of the graphene sheets (making holey graphene and h-graphene) to release these impurities and reconstruct the graphene network's hexagonal structure after suitable heat treatment (Chen et al. 2019).

Along with its mechanical and electrical properties, we must also consider its biocompatibility, which makes rGO usable in the biomedical field as biosensors.

Another interesting application of rGO is manufacturing fibers. Qu et al. were among the first to propose a manufacturing method using a suspension of GO in water (Dong et al. 2012). Their very simple technique involved heating a suspension of GO (8 mg GO/mL) contained in a glass tube (inner diameter 0.4 mm), closed at both ends, at 230°C for 2 h. This produced fibers with diameters of 150 µm when wet and only 35 µm when dry.

From a mechanical point of view, the stress–strain curves considerably improve after heat treatment at 800°C for 2 h under argon, increasing the tensile strength from 120 to 420 MPa. The electrical conductivity of these fibers is 10 S/cm, like fibers made from CNTs. It is easy to knot or twist the fibers, illustrating their great flexibility (Figure 1.13).

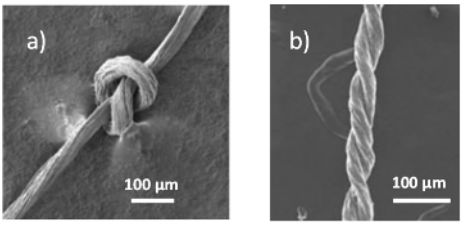

Figure 1.13. *SEM images of graphene fibers. (a) Knot formation; (b) two-strand twisted graphene fiber. Adapted from Dong et al. (2012)*

Given the technological importance of these fibers, many teams have become involved in this field of research to produce graphene fibers with properties as close as possible to those of default-free monolayer graphene films.

Gao's group recently continuously produced very high-quality graphene fibers on a large scale (Xu et al. 2016). The high quality was due to the optimal orientation of the GO micro-sheets. Initially obtained as a dispersion in water (from 1 to 10 mg of GO/mL in solution), the GO dispersion was then transferred into a solution of N,N dimethyl formamide (DMF), which has the effect of creating a liquid crystal structure with the GO micro-sheets in a parallel arrangement. The fibers were extruded through a small diameter die (60 µm) and then wound onto a spool using rotating cylinders. Heat treatment under nitrogen at 3,000°C transforms the GO fibers (GOFs) into graphene fibers (GFs). These GFs have very good mechanical properties as well as very good electrical and thermal conductivities. Their Young's elasticity modulus is between 385 and 400 GPa (measured with a 5 mm long wire), and their ultimate tensile strength is around 1.8–2.2 GPa. Conductivity at room temperature reaches up to 0.8×10^6 S/m and is independent of the length of wire tested; the ampacity is extremely high and corresponds to current densities of 2.3×10^{10} A/m^2. These values are comparable and sometimes better than those measured with wires formed from CNTs.

This large-scale production of extremely flexible and mechanically resistant GFs, whose electrical properties are comparable to those of metals, such as copper, but with very low mass densities, makes them suitable for numerous applications. The authors thus demonstrate how graphene fiber winding can replace copper wires in the manufacture of an electric motor, with a significant mass advantage,

considering the differences in density between GFs (0.23 g/cm^3) and copper wires (8.96 g/cm^3) (Dong et al. 2012).

In parallel with this work, the same group showed that the conductivity of GFs could be greatly increased when doped with certain elements. Liu et al. (2016) obtained GFs with conductivities of 0.77×10^7 S/m (GF-$FeCl_3$), 1.5×10^7 S/m (GF-Br_2) and 2.24×10^7 S/m (GF-K), values close to those of copper (~6×10^7 S/m to 20°C).

1.1.5.3.3. Graphene-polymer nanocomposites

The idea of using a small amount of graphene to significantly improve the mechanical, electrical and thermal properties of composite polymers is attractive. Ruoff and his research group were the first to investigate this concept, starting with GO nanoparticles (GO-NPs) dispersed in water to develop large-scale polymer composite materials (Stankovich et al. 2006).

The main obstacle to overcome is that the graphene nanoparticles (G-NPs) inserted into the polymer matrix are generally obtained by reducing GO-NPs, also dispersed in water. After reduction, the G-NPs immediately aggregate together, given the hydrophobic nature of the nanoparticle core. This makes it difficult to individually insert G-NPs into a polymer solution because most polymers are insoluble in water. The solution proposed by Ruoff et al. involves making the GO-NPs less hydrophilic by transforming the OH and COOH groups of the GO sheets into amide and carbamate functional groups, which are weakly hydrophilic. Exfoliation is no longer possible in an aqueous medium but readily occurs in an aprotic solvent like DMF. The authors obtained a dispersion of functionalized graphene oxide nanoparticles (fGO-NPs) in an organic medium, where numerous polymers can be solubilized. Astonishingly, the reduction of fGO-NPs by hydrazine in the presence of a polymer such as polystyrene only leads to an aggregation of the G-NPs and the polymer and not to an aggregation of NPs, ultimately forming a graphene–polymer composite.

Since this initial research, many teams have invested in this area of research and made numerous improvements and modifications to the graphene–polymer composite manufacturing process. Several articles have been published on this topic (Potts et al. 2011; Das and Prusty 2013; Hu et al. 2014a; Bera and Maji 2017; Malucelli 2017), which provide details of the composites obtained for many polymers of technological interest and the variations in manufacturing methods, including the functionalization of G-NPs, which have led to significant improvements on a mechanical and electronic level. Numerous applications exploited graphene–polymer composites in the design of biosensors, as described in the review article by Yusaf et al. (2022).

1.1.5.3.4. Conclusion

Graphene is one of the few materials that exhibit exceptional electrical and thermal conductivity, resist extremely high temperatures and high current densities greater than those of the most conductive metals such as copper. They also have mechanical properties such as elasticity and tensile strength far exceeding those of steel and a low mass density of 0.23 g/cm^3. Such properties have only been obtained for mechanically exfoliated graphene sheets, which are defect free and can only be obtained in very small quantities, making it unrealistic to imagine large-scale production.

CVD methods have evolved considerably and can now continuously produce good-quality graphene ribbons. However, this technique requires large equipment that can only be used in an industrial setting. On the other hand, the chemical transformation methods of GO into G prove to be easier to access and have progressed considerably too. GO, obtained in large quantities by the simple oxidation of graphite, is the precursor to graphene, which can be obtained in large quantities and various forms. Graphene can be produced as very long, highly homogeneous fibers a few micrometers in diameter and can even be used to manufacture composite materials. The quality of the graphene produced is considerably improved by heat treatment at very high temperatures in an inert atmosphere, which restores its graphitic structure.

Given these properties, graphene's potential areas of application are vast (Figure 1.14), falling under the following: energy (storage and conversion), biomedicine (medical imaging and vectorization of drugs), electronic devices (sensors, transistors, electrodes, electromagnetic shielding) and mechanics (artificial muscles).

The cost of graphene, however, remains high and its price, which varies greatly, fluctuates between 100 and 300 USD per gram. Furthermore, it is also available in the form of sheets adsorbed onto a Si/SiO_2 substrate, making it possible to directly manufacture various sensors. Fortunes business estimated the graphene market at 430 million USD in 2023, reaching an expected 2.96 billion USD in 2030. This represents a compound annual growth rate (CAGR) of 31.6% for this period[20].

20 Researchers at Rice University proposed significantly lowering the cost of graphene thanks to a new process called "flash graphene" (FG), which involves irradiating ordinary carbon sources at 2,700°C for 10 ms. They believe it is possible to obtain 1 g of the FG product with high purity while consuming little electrical energy, equivalent to 7.2 kJ (Luong et al. 2020).

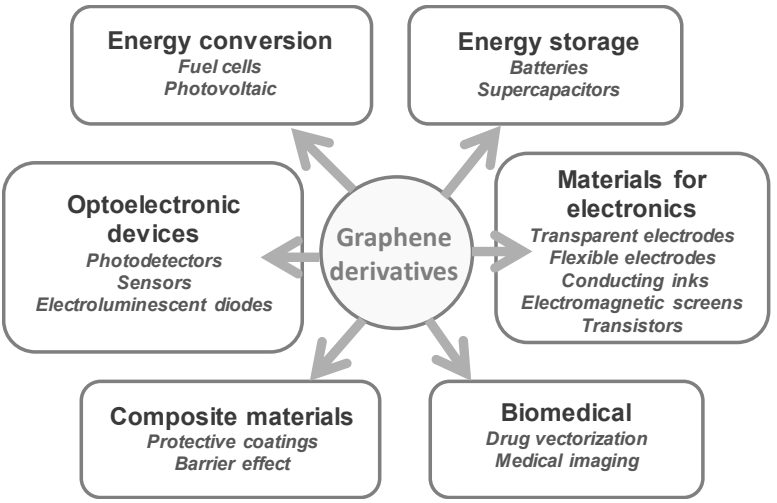

Figure 1.14. *Implications of graphene derivatives in different fields. For a color version of this figure, see www.iste.co.uk/lacaze/nanotechnologies.zip*

1.1.6. *Graphene quantum dots*

Graphene quantum dots (GQDs) are nanometric-sized graphene fragments like point nanoparticles (0 D) with characteristics similar to graphene and CQDs. As for CQDs, one should expect quantum confinement effects, edge effects and some structural properties characteristic of graphene. Less than 10 nm in size and less than 10 layers thick, GQDs are fluorescent materials due to the confinement effect. Unlike graphene, GQDs have a non-zero band gap, making them semiconductors and suitable for applications in optoelectronics.

1.1.6.1. *GQD manufacture methods*

Novoselov et al. first manufactured GQDs by CNT fragmentation in 2008 (Ponomarenko 2008), and many techniques have since been proposed. These techniques have been classified into two main categories: top-down and bottom-up. Top-down techniques involve cutting fullerenes, CNTs, carbon fibers or graphene into fragments, while bottom-up techniques involve synthesizing GQDs by chemically transforming carbon molecules (precursors). Citric acid, glucose or other compounds containing benzene rings have been used as precursors for manufacturing GQDs (Valappil et al. 2017; Tian et al. 2018).

The fragmentation of a carbon-based material, preferably with aromatic nuclei, is frequently used in top-down methods. Graphite is preferred, but other materials, such as cotton fibers, have also been transformed into GQDs (Zuo et al. 2017). For

example, chemically transforming graphite in an acidic environment together with microwaves produces large quantities of GQDs and does not require large logistical investments. This was the method used by Luo et al. (2016) to obtain emissive GQD films used in white light-emitting diodes.

Unlike previous methods, bottom-up methods can produce GQDs from growth reactions of carbon compounds and form condensed aromatic structures by thermolysis in an aqueous medium. The carbon precursors can be polycyclic aromatic compounds (pyrene, 1,5-dinitro naphthalene) or non-aromatic compounds.

Bottom-up methods have the undeniable advantage of simplicity when obtaining GQDs doped with elements other than carbon. Nitrogen-doped GQDs (N-GQDs) can be produced in a single step by directly treating a mixture containing a nitrogen derivative and the carbon precursor. Nitrogen-doped nanomaterials have significantly better photoluminescence (PL) properties than undoped GQDs and are particularly interesting for medical imaging due to their luminescence properties, high stability in an aqueous medium and their non-toxicity. They have also found other applications in the energy and sensors fields (Kaur et al. 2018).

Through the thermolysis of citric acid in ethylene diamine, Yang and his colleagues obtained N-GQDs sized between 5 and 10 nm with thicknesses between 0.8 and 2.5 nm, the equivalent of two to five superimposed layers. Curiously, the high internal quantum yield of the blue PL obtained with these N-GQDs, around 75%, far exceeds the quantum yields usually observed with this type of materials (Gu et al. 2016).

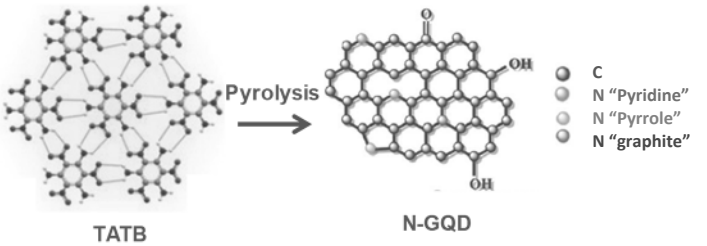

Figure 1.15. *Obtaining N-GQDs by pyrolysis of TATB. The TATB precursor is made up of a supramolecular planar network of TATB molecules linked by hydrogen bonds between the H of the NH_2 and the O of the NO_2 (the red and blue spheres represent the oxygen and nitrogen atoms, respectively, and the gray spheres, the carbons). In the N-GQD, the nitrogen atoms are incorporated into the graphitic network and occupy different positions corresponding to different functionalities (pyridine, pyrrole or graphite). Adapted from Li et al. (2016a). For a color version of this figure, see www.iste.co.uk/lacaze/nanotechnologies.zip*

Another way to obtain N-GQDs is to start from a single compound like 1,3,5-triamino-2,4,6-trinitrobenzene (TATB), which has carbon and nitrogen necessary for forming N-GQDs (Li et al. 2016a). A pyrolysis reaction at a high temperature (750°C for approximately 20 min) in a nitrogen atmosphere synthesizes N-GQDs with good yields. The doping rate atomic value of nitrogen is about 10% compared to carbon atoms (Figure 1.15).

1.1.6.2. *Properties and applications of GQDs*

GQDs, unlike graphene, have a non-zero forbidden energy band, the width of which depends on the size, shape and edge effects of these nanoparticles. Given the great diversity of GQDs and their lack of homogeneity in size and shape, their optoelectronic and photoemission properties closely depend on the abovementioned parameters. Photoemission is one of the main properties of GQDs, exploited in various detection systems, particularly in medical imaging.

The PL of GQDs is controlled by the nanomaterial core (which may be assimilated to a graphene fragment), the surface states corresponding to functional groups positioned at the ends of the nanoparticles and the heteroatoms incorporated after doping. Like CQDs, the fluorescence emission of GQDs strongly depends on the excitation wavelength (Figure 1.16).

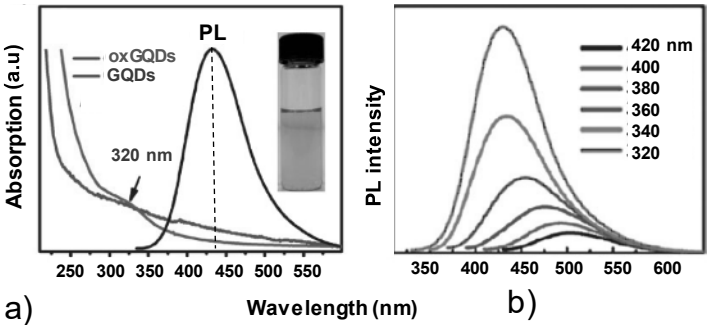

Figure 1.16. *Photoluminescence (PL) intensity curves of GQDs as a function of excitation wavelength. (a) Absorption curves of GQDs and oxidized GQDs (oxGQDs) and PL curves resulting from the excitation of GQDs at 320 nm. Visible light photographs of an aqueous solution of GQDs. (b) PL intensity curves emitted for excitation wavelengths between 320 and 420 nm. Adapted from Pan et al. (2010). For a color version of this figure, see www.iste.co.uk/lacaze/nanotechnologies.zip*

Zhu et al. (2014), in a very detailed spectroscopic study (static and dynamic), showed that the photoemission properties of GQDs are determined by the relative position of the GQD intrinsic energy (IE) levels and the energy levels due to edge

effects (EE). IE energy levels correspond to the energy of the orbitals π* in graphene fragments and the EE levels to the functional groups grafted to the edge of the GQDs.

Using GQDs of increasing size ($C_{42}H_{18}$–1.2 nm, $C_{96}H_{30}$–1.9 nm, $C_{132}H_{34}$–2.5 nm), the authors show that the energy of the intrinsic transition π→π* decreases with the GQD size along with the energy difference ΔE between IE (π*) and EE levels. The energy difference ΔE determines the nature and intensity of the luminescence, which originates from the deactivation of the EE state. The emission is fluorescence for a non-zero ΔE and can be combined with phosphorescence when ΔE is zero. The fluorescence intensity can be very weak or absent when the IE and EE energy levels are similar, which is observed in GQDs with formulas $C_{132}H_{34}$ and $C_{222}H_{42}$ (Zhu et al. 2014) (Figure 1.17).

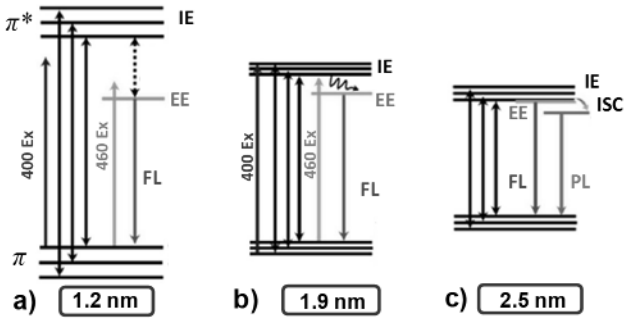

Figure 1.17. *Interpretation of the photoluminescence of GQDs according to their size and luminescence excitation energy. (a) GQD ($C_{42}H_{18}$, size 1.2 nm): excitation at 460 nm only gives fluorescence emission. (b) GQD ($C_{96}H_{30}$, size 1.9 nm): the two excitations at 400 and 460 nm, after energy transfer from IE (intrinsic energy state π*) toward EE (energy level due to functional groups located on the edges of the GQD) emit high-intensity fluorescence FL. (c) GQD ($C_{132}H_{34}$, size 2.5 nm): EE merges with IE; possible intersystem crossing (ISC) of IE toward its triplet state simultaneously emits fluorescence and phosphorescence PL. Adapted from Zhu et al. (2014a). For a color version of this figure, see www.iste.co.uk/lacaze/nanotechnologies.zip*

Recent years have seen the development of many research studies proposing the use of GQDs for energy and biomedical applications. In the field of energy, GQDs can significantly improve the operation of battery electrodes and the performance of supercapacitors. Their PL properties have also been used to improve the operation of OLEDs and some photovoltaic devices since they can intervene favorably in photocatalytic processes. GQDs have found the most potential applications in the

biomedical field, including biomedical imaging, vectorized drug delivery, various forms of phototherapy, antibacterial products and biosensors (Kumar et al. 2020).

1.2. Inorganic nanomaterials

The metals Au, Ag and their alloys, one of the largest families of inorganic nanomaterials currently studied, have by far the most studies devoted to them, followed by oxides (TiO_2, MnO_2, Fe_3O_4) and chalcogenides (CdS, CdSe and Bi_2Te_3). The latter are involved in manufacturing QDs due to their semiconductor properties (Figure 1.18) (Portehault et al. 2018).

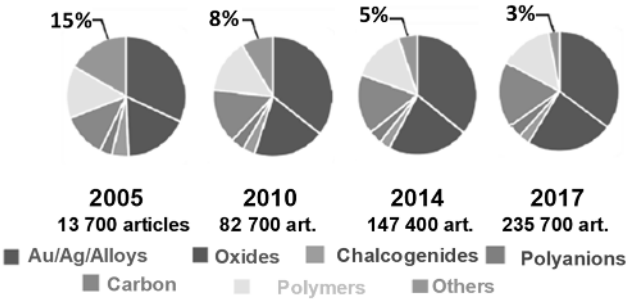

Figure 1.18. *Cumulative progression of the number of articles published on the different types of NPs between 2005 and 2017. Adapted from Portehault et al. (2018). For a color version of this figure, see www.iste.co.uk/lacaze/nanotechnologies.zip*

COMMENT ON FIGURE 1.18.– *The number of publications devoted to noble metals and oxides increased continuously between 2005 (around half of the total) to two-thirds of the number of publications in 2017. Publications on materials other than carbon derivatives, polymers and inorganics declined significantly from 15% to 3% during the same period; those concerning chalcogenides and polyanions remained unchanged and formed only a small part of all publications*.

All these nanomaterials can be easily functionalized with organic molecules or polymers, making them soluble in aqueous environments in the form of colloids and sensitive to their environment. It also gives them suitable transport and vectorization properties for biomedical applications. They can also be organized into lattices, giving them new properties such as plasmon resonance and exaltation phenomena, mainly observed in the UV-visible spectral range for gold and silver.

1.2.1. *Metal nanoparticles*

Many studies have been devoted to the NPs of noble metals, particularly gold, due to the vast potential applications in analytical chemistry, catalysis, in developing optoelectronic devices, and, due to their safety, in the biomedical field.

The properties of metallic NPs as well as their preparation methods have been the subject of numerous studies, reviewed in the mid-2000s by the Astruc (Daniel and Astruc 2004) and El Sayed (Eustis and El-Sayed 2006) groups. More recently, the Jin and Gilroy groups also discussed metal nanoclusters (NCs) and bimetallic nanocrystals and other specific domains of NPs (Gilroy et al. 2016; Jin et al. 2016). Producing monodisperse NPs with a controlled shape and accurately defined physicochemical criteria for good reproducibility are among the main challenges of current research. There are currently two contending techniques for preparing these nanomaterials. The most widespread and accessible is the chemical preparation of colloidal NP solutions by reducing metal salts in an aqueous medium with surfactants. Other methods, more extensive in terms of equipment and well known to physicists, are based on laser ablation techniques for materials in the gaseous state or solution (Kortshagen et al. 2016) and, more recently, on sputtering techniques for metallic materials (Ishida et al. 2017), well suited for the manufacture of metallic NCs.

1.2.1.1. *Gold nanoparticles*

This is an area of research that has given rise to the greatest number of publications, most of which have been devoted to studying the growth mechanisms of gold NPs and the techniques for producing them. The main challenge has been selecting the physicochemical parameters, which will allow control of the NP size and morphology.

In the 1950s, Turkevich et al. (1951) were the first to propose a precise protocol for obtaining "citrated" spherical gold NPs with controlled sizes by reducing Au^{3+} ions in an aqueous solution using trisodium citrate[21]. The Au^{3+} ions are solubilized in water in the form of the tetrachloroauric acid complex ($HAuCl_4$) and the citrate is gradually added to the Au^{3+} ion solution to produce a double effect: on the one hand, it reduces the Au^{3+} ions to the Au° metal state, and on the other hand, it stabilizes the formed NPs by adsorbing to their surface, resulting in the formation of a stable colloidal solution of gold NPs dispersed in water. The concentrations of the reagents

21 Gold in a divided form has been used as a color pigment since ancient times. Only in the form of nanospheres was it used and mixed with different materials such as glasses and polymers, and it was Michael Faraday (1850) who was the first to recognize that their colors were due to their extreme divisions.

are decisive for obtaining spherical NPs of a determined size. The reaction mechanism involves several stages of reduction and complexation, later the subject of various interpretations (Kumar et al. 2006).

Different techniques have been developed to increase the monodispersity of metallic NPs. The seed-mediated growth technique, where NPs are grown from nucleation seeds, was developed by El Sayed and Murphy and their teams, and adopted by numerous groups. Developing various shapes (rods, cubes, discs, rectangular or triangular platelets, etc.) has become possible thanks to these nucleation seeds (Figure 1.19).

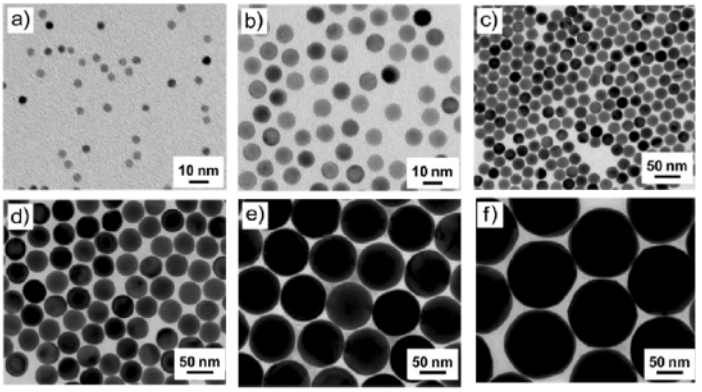

Figure 1.19. *Transmission electron microscopy (TEM) images of gold NPs of different sizes. (a) 5 nm, (b) 10 nm, (c) 23 nm, (d) 46 nm, (e) 100 nm and (f) 150 nm. According to Zheng et al. (2014b)*

Spherical gold NPs with controlled sizes between 5, 10, 30, 50, 100 and 150 nm were also synthesized using this method by injecting increasingly larger gold seeds into tetrachlorauric ($HAuCl_4$) acid solutions, together with ascorbic acid as a reducing agent (instead of citrates) and a surfactant such as cetyltrimethylammonium chloride (CTAC). Gold NPs of approximately 30 nm in diameter are made using seeds of 10 nm gold NPs; the 30 nm gold NPs can then be used as seeds to obtain larger NPs, and so on until NPs of 150 nm are obtained. Producing NPs in the form of nanorods (NRs) began with El Sayed (Huang and Wan 2009) and Murphy (Sau and Murphy (2004) in the 2000s and has also been the subject of numerous studies. The anisotropic growth technique using nucleation seeds makes it relatively easy to produce gold NPs, but the experimental conditions differ from those defined for obtaining nanospheres. Such a mode of growth has been described by Song and his collaborators using gold decahedrons as seeds,

synthesized in the presence of high concentrations of poly(vinylpyrrolidone) compared to that of $HAuCl_4$ (Seo et al. 2008, 2009) (Figure 1.20).

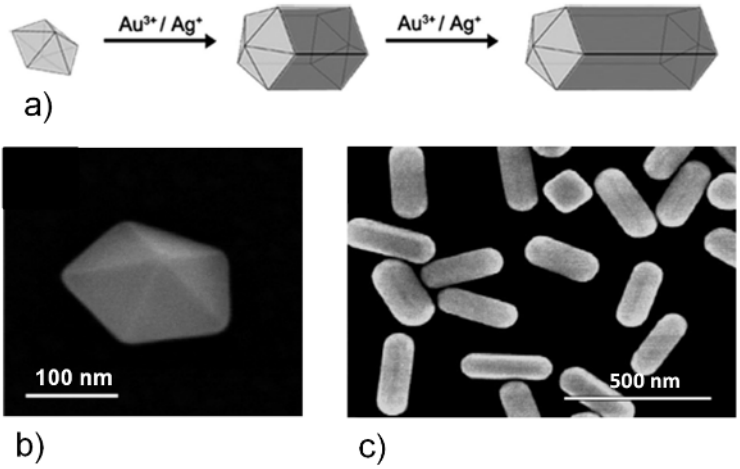

Figure 1.20. *SEM images of NRs obtained from decahedral seeds. (a) Schematic diagram of the NR growth from decahedral seeds in the presence of silver salts. Ag^+ ions are known to block the crystal faces of gold nanopolyhedra and promote the anisotropic growth of NRs. (b) SEM image of a large gold decahedron (80 nm). (c) SEM images of NRs obtained from gold decahedra whose edges have average lengths of 60 nm. (a and c) Adapted from Seo et al. (2009); (b) according to Seo et al. 2008)*

This method of growing gold NPs from metal seeds has made it possible to produce varied forms of NPs and is applicable to many metals besides gold. Numerous variations in the method have also been proposed and varying forms of gold NPs have been obtained. These are described in the review article by Xia et al. (2017) together with the other metals produced via this method.

The optical and physical properties of NRs depend on their dimensions and particularly on their aspect ratio, defined as the length/width ratio, due to their elongated shape. The higher the aspect ratio, the more the light absorption is shifted toward the red, which corresponds to a shift in the plasmon resonance of these NPs toward lower frequencies (Eustis and El-Sayed 2006). Gold NPs are widely used in sensor applications because their optical extinction spectrum closely depends on the environment surrounding them. The sensor applications of gold NPs, based on their plasmonic properties, will be discussed in Chapter 4.

1.2.2. *Metal nanoclusters (MNCs)*

These are very small NPs, aggregates of atoms (between 10 and 300 atoms), whose diameters are between a fraction of a nm and a few nm (maximum 2.2 nm)[22]. Compared to larger NPs (beyond 10 nm), the optical properties of MNCs vary even for very small fluctuations in size (1 Å), whereas for NPs bigger than 10 nm, their optical properties are little affected when size variations of 1 nm occur. This is because, as soon as we reach dimensions less than 2–3 nm, the quantum effect due to confinement causes the band structure characteristic of metal in the bulk state to be replaced by discrete energy levels analogous to those of an atom or molecule. In the case of large NPs, the absorption of light corresponds to a plasmon resonance of the electrons located in the conduction band (see Chapter 4), while for very small NPs the absorption of light corresponds to electronic transitions between occupied (highest occupied molecular orbital [HOMO]) and vacant energy levels (lowest unoccupied molecular orbital [LUMO]).

The field of MNCs is vast, but it is gold (AuNCs) and silver (AgNCs) NCs that have found the greatest applications, mainly due to their fluorescence properties (Russier-Antoine et al. 2014). Since the 2000s, the luminescence of gold NPs has been demonstrated with AuNCs sized between 1 and 2 nm, with very low quantum yields (between 10^{-5} and 10^{-3}) (Zheng et al. 2012). These low quantum yields appear to be the general rule for most AuNCs stabilized by thiolated ligands.

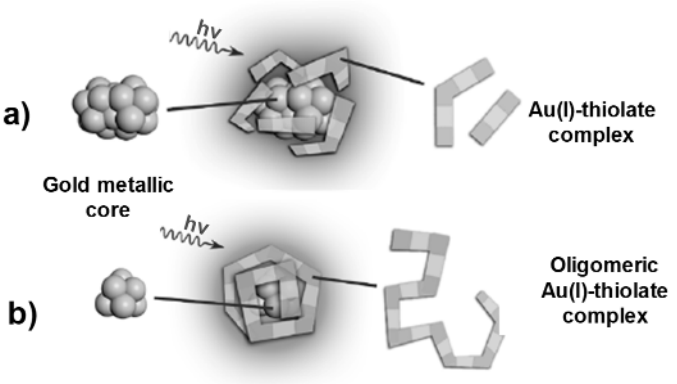

Figure 1.21. *Comparative luminescence of gold NCs chelated by simple Au(I)-Thiolate complexes or by oligomers of the Au(I)-thiolate complex. (a) UV excitation (360 nm) of the Au(I)-thiolate complex does not induce any luminescence. (b) Excitation under the same conditions of the Au(0)@Au(I)-thiolate NC complex induces strong luminescence around 600 nm (orange). Adapted from Luo et al. (2012). For a color version of this figure, see www.iste.co.uk/lacaze/nanotechnologies.zip*

22 The word nanocluster describes very small atomic aggregates.

Thanks to the development of new preparation methods, luminescence quantum yields of over 10% were then achieved by Xie and his team, by producing core-shell structures in the case of Au_{25}-NCs complexed with glutathione (GS) ligands (Luo et al. 2012). According to the authors, this increase in quantum yield corresponds to a new phenomenon of luminescence known as aggregation-induced emission (AIE)[23] resulting from the aggregation of emissive units transformed into oligomers around the metal core (Figure 1.21). This increase in luminescence compared to conventional AuNCs is interpreted by Luo et al. as the consequence of a stiffening of the NC, weakening all non-radiative deactivation processes.

These results apply to a whole series of ligands with one atom (sulfur, nitrogen, etc.) capable of firmly attaching to a metal core of atoms. The quantum yields observed with different gold NCs, listed in several review articles, vary between 1% and several tens of percentage. Very high quantum yields (from 10 to 70%) were obtained by complexing AuNCs with poly(amidoamine) dendrimers. Dickson and his team observed luminescence emissions ranging from UV-visible for the smallest sizes to near-IR for the largest (Zheng et al. 2004).

AuNCs are currently considered luminescent materials particularly suited to the analysis and detection of metal ions, molecules of biological interest, proteins, and nucleic acids, as well as the fluorescent labeling of biological molecules used in imaging. Their ease of preparation and functionalization, the emission of a stable and intense luminescence and color that can be easily modulated according to the size of the MNCs, their good biocompatibility and their absence of toxicity constitute many favorable properties, which have found many applications in the detection and analysis of metal ions and biological molecules, as reported in the review article by Halawa et al. (2018a).

1.2.3. *Semiconductor QDs*

The 2023 Nobel Prize in Chemistry was awarded to Moungi Bawendi, Louis Brus and Aleksey Yekimov for developing semiconductor QDs. Their discovery and

23 This AIE effect was described in the 2000s by Tang and team by comparing the luminescence of 1-methyl-1,2,3,4,5-pentaphenylsilole in solution and in the solid state (Luo 2001). In solution in alcohol, the luminescence quantum yield is very low (0.6×10^{-3}), whereas in the form of a solid film, the luminescence quantum yield is 0.2, an increase of more than 300 times. This increase in luminescence is due to a greater flatness resulting from the formation of aggregates and stronger electron conjugation. Note that this enhanced luminescence phenomenon by the aggregation of emissive units is unique and opposes the accepted general law, which states that the condensed state leads instead to the extinction of fluorescence.

the ability to synthesize such materials with simple chemical methods was an important stage in the evolution of nanoscience and nanotechnology[24].

Considered to be semiconductor NCs, resulting from binary, ternary and multinary combinations of different elements, they are a family of inorganic nanomaterials less than 10 nm in size. Over the last two decades, they have been the subject of many studies, focusing on their preparation techniques and physicochemical properties. Essentially, their fluorescence is used in biomedical imaging, electroluminescence applied to LEDs (light emissive diodes), television display screens, photovoltaics, etc. (Kovalenko et al. 2015).

Figure 1.22. *Photoluminescence of some QDs showing that their color emission domains cover the entire visible range. For a color version of this figure, see www.iste.co.uk/lacaze/nanotechnologies.zip*

Semiconductor QDs are characterized by a band gap that varies depending on their size and composition, which gives color emissions ranging from UV-Visible to IR and far-IR. The most typical QDs are binary combinations of elements belonging to columns II and VI of the periodic table, corresponding to metal chalcogenides (CdS, CdSe, ZnS, ZnSe, PbS, TeS, etc.). However, an evolution has occurred toward ternary and quaternary combinations of metals that are much less toxic and correspond to combinations of type I-III-VI_2, ($CuInS_2$, CIS; $CuIn_{1-x}Ga_xSe_2$, CIGS corresponding to chalcopyrites) and I_2-II-IV-VI_4 (Cu_2ZnSnS_4, CZTS corresponding to kesterites), whose band gap, well adapted to the solar spectrum, are well suited for photovoltaic applications.

QDs are typically characterized by broad excitation bands, narrow fluorescence emission peaks and high intensities. Their quantum yields are comparable to those of organic fluorophores but their extinction coefficients are 10 to 50 times larger.

24 Available at: https://www.nobelprize.org/prizes/chemistry/2023/press-release/.

This strong propensity to absorb light makes them ideal candidates for use in energy conversion systems. Unlike organic fluorophores, they are more chemically stable and resist photobleaching (loss of fluorescence during irradiation), 100 times better than that of organic molecules (Yao et al. 2014).

The first colloidal solutions of QDS such as CdS and CdTe were synthesized in the 1980s, where the QDs were stabilized by the adsorption of organic molecules, but high fluorescence yields were not obtained. In the 1990s, significant progress toward controlling the dimensions of CdS, CdSe and CdTe NCs was made (Murray et al. 1993). Subsequently, synthesis methods producing large quantities of QDs were proposed in the 2000s. Cao and his group (Yang et al. 2005) thus developed a method for synthesizing CdSe based on the reaction of a mixture at high temperature of two precursors (Myristate of Cd and Se) in solution[25].

Their stability with respect to the external environment can be considerably improved using core-shell structures, such as ZnS@CdSe, where the fluorescent QD (CdSe) is covered by a SC layer, such as ZnS, with a band gap much greater than CdSe (Kortan et al. 1990). Unfortunately, this strategy makes the fluorescence of QDs insensitive to their environment and hence unsuitable for sensor applications.

Currently, the techniques for preparing QDs via the colloidal route have made considerable progress. It is now possible to produce large quantities of QDs at costs compatible with their commercialization, covering a whole range of wavelengths, from visible to near IR (NIR; Bang et al. 2017; Owen and Brus 2017; Pu et al. 2018b). Lead-based QDs that fluoresce in the NIR are particularly important for applications in biomedical imaging.

In conclusion, colloidal QDs are currently considered nanomaterials with exceptional fluorescence properties, including emission wavelengths that vary depending on their size, high quantum yields and pure color emissions. They are also chemically stable and resistant to photobleaching, unlike organic fluorophores. They can be prepared on a large scale and at low cost. These properties make QDs particularly suitable for display and lighting applications requiring electroluminescence. Their luminescence properties make them attractive in sensor applications, for which different emission and quenching mechanisms by resonance energy transfer can be considered for analytical purposes (see Chapter 4).

---

25 Cd Myristate (Cd salt of tetradecanoic acid – $CdC_{28}H_{54}O_4$) decomposes at 226°C; Selenium powder has a melting point of 221°C and becomes slightly soluble in a solvent such as 1-octadecene (ODC-$C_{18}H_{36}$) beyond 190°C. By choosing a reaction temperature of 240°C, QDs can be obtained with very good monodispersity (size differences less than 5%) and very good fluorescence properties (quantum yield around of 30–40%) (Yang et al. 2005).

1.2.4. *Two-dimensional inorganic lamellar nanosheets*

Graphene has extraordinary conductivity properties due to its two-dimensional lamellar structure. Since its discovery, there has been renewed interest in other 2D inorganic materials (2DMs) with similar lamellar structures, such as transition metal dichalcogenides (TMDs) and some oxides and hydroxides, since it was shown that they could be obtained in the form of two-dimensional nanosheets with one or more atomic layers. Strano et al. nicely described the optoelectronic properties and applications of the main TMDs formed of MoS_2, $MoSe_2$, WS_2 and WSe_2 nanosheets (Wang et al. 2012).

Alongside the vast family of bidimensional TMDs, other lamellar materials such as tin sulfide (SnS_2) (Qu et al. 2014), and phosphorene, a semiconductor made of an assembly of black phosphorus (BP) atoms can also be exfoliated into nanosheets. Also, hexagonal boron nitride (hBN), a two-dimensional material isomorphic to graphene but insulating, is another 2D material structured as a hexagonal network of boron and nitrogen atoms (Zhang et al. 2017a).

Finally, a new family of 2DMs, called MXenes, was discovered in 2011 by Gogotski et al. (Naguib et al. 2011). They have the generic formula $M_{n+1}X_nT_x$, where M is a transition metal, X is a carbon or nitrogen atom, and T is an OH, O, or F group. Also considered as transition metal carbides or nitrides, they have very good conductivity and are often compared to graphene. Their properties depend on the nature of the surface Tx terminations.

1.2.4.1. *Dichalcogenides*

Unlike graphene, which is formed only of carbon atoms, the great chemical diversity of TMD atoms gives a much wider range of properties, including materials that can be semiconductors (MoS_2 and WS_2), semi-metallic (WTe_2 and $TiSe_2$), metallic (NbS_2 and VSe_2) and superconductors ($NbSe_2$ and TaS_2) (Lv et al. 2015). Furthermore, depending on the number of layers and composition, semiconductor TMDs can have a direct or indirect energy band gap and n or p-type charge carriers (Chhowalla et al. 2013, 2015). These properties have opened the field to catalysis, energy storage and electronics applications. New field effect transistors (FETs) have been made from TMDs and used for analytical purposes to detect chemical compounds and create optoelectronic devices and new logic circuits, as described in several review papers (Tan and Zhang 2015; Anichini et al. 2018; Xiong et al. 2019).

Metallic dichalcogenides such as molybdenum sulfide (MoS_2), tungsten sulfide (WS_2) and titanium sulfide (TiS_2) are the most widely studied, with MoS_2 being considered the most accessible (Anichini et al. 2018). Unlike graphite, formed by

the stacking of identical graphene layers, TMDs comprise an assembly of hybrid layers in which a layer of a transition metal M is arranged like a "sandwich" and linked covalently to two outer layers of sulfur atoms. The external planes of these hybrid layers are held together by Van der Waals forces, which explains (as for graphite) their easy separation in exfoliation techniques (Figure 1.23).

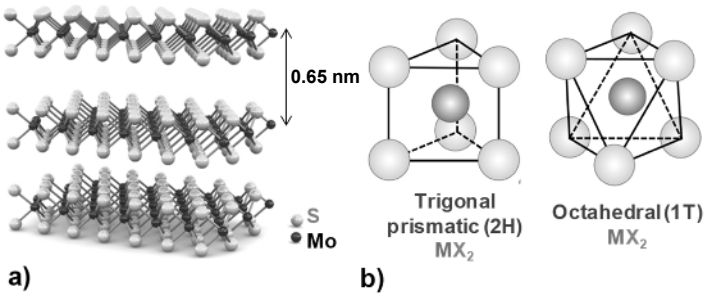

Figure 1.23. *Representation of the crystal structures of TMDs (MX2 structure). (a) Three-dimensional representation of the different planes of a MoS_2 crystal (distance between two 0.65 nm layers). According to Radisavljevic et al. (2011). (b) Representation of the two crystal forms 2H (trigonal) and 1T (octahedral, the most stable). According to Lv et al. (2015). For a color version of this figure, see www.iste.co.uk/lacaze/nanotechnologies.zip*

Two main methods are used to produce these nanosheets: exfoliation of the material from the bulk state or CVD. The first is an electrochemical reaction, lithium-ion intercalation-based exfoliation, where Li+ ions are intercalated into the bulk of TMD using a similar mechanism to that found in a lithium battery. After the intercalation of lithium, the product obtained is subjected to sonication, which releases dihydrogen, causing TMD to disintegrate and nanosheets to form, collected as a suspension in water with a yield greater than 90% (Huang et al. 2013). The same direct sonication process can be used to cause the disaggregation of TMDs with a solvent such as N-methylpyrrolidone, which exhibits good wettability with the TMD. MoS_2, WS_2, $MoSe_2$, $NbSe_2$, $TaSe_2$, $NiTe_2$, $MoTe_2$, h-BN and Bi_2Te_3 nanosheets with one or more atomic layers can be prepared according to this method.

The second method for preparing TMDs and CVD produces large lateral crystals with controlled thicknesses of one or more atomic layers. MoS_2 nanosheets are obtained by heating sulfur and MoO_{3-x} precursors in powder form. Sulfur in the vapor state reacts with the sub-oxide $MoO_{3-x,}$ forming MoS_2 condensed as a film on a Si/SiO_2 substrate. Numerous variations in the choice of precursor have been proposed, making it possible to obtain large nanosheets.

TMDs, particularly MoS_2, have interesting properties. Easy surface functionalization by metals and modification of their composition by doping or forming alloys; hybrid nanostructures can also be synthesized by combining TMDs nanosheets with carbon-based or inorganic nanomaterials (Tan and Zhang 2015). TMD nanocomposites doped on the surface by precious metals (Pt, Pd, Au, Ag) or alkalis, TMD alloys of the $MoS_{2(1-x)}Se_{2x}$ and $Mo_{1-x}WxS_2$ type, or assemblies between TMD and graphene, CNTs or carbon fiber nanosheets have been fabricated.

Doping with a metal chemisorbed to the surface of a TMD modulates the electronic properties of TMDs. MoS_2 and WSe_2 nanosheets doped with potassium can be transformed into degenerate n^+ semiconductors, characterized by very high surface electron densities (respectively, ~$10^{13}/cm^2$ and $2.5 \times 10^{12}/cm^2$ for MoS_2 and WSe_2) (Fang et al. 2013). FETs with very good electrical characteristics can be formed with a channel made of MoS_2 or WSe_2 nanosheets, whose extremities in contact with the electrodes (source and sink) are n^+ doped. One advantage of MoS_2 or $WeSe_2$ nanosheets over silicon is that their surfaces are extremely homogeneous, and the thicknesses of the nanosheets are perfectly uniform over the entire area.

In summary, TMD nanosheets are a new family of 2D nanostructures that are easy to produce and functionalize. Their electrical and photonic properties make them potential competitors of all other 2D nanomaterials, requiring more difficult production conditions. Their semiconductor properties make them more operational than graphene for the design of transistors. The few application examples described in this section show that their application prospects are immense and have already brought significant achievements in plastic electronics, energy and analytical chemistry with the design of innovative sensors using FETs (see Chapters 4–6).

1.2.4.2. *MXenes*

MXenes have the general formula $M_{n+1}X_nT_x$, where M is a top-row transition metal (Ti, Sc, V, etc.), X carbon or nitrogen and T is the terminating surface groups corresponding to groups OH, F, Cl, and =O. MXenes are obtained from lamellar 3D materials with the general MAX structure, comprising alternating MX and A sheets strongly bonded to each other (A is generally aluminum [Al]). Unlike other TMD materials, such as 3D chalcogenides, for which van der Waals forces weakly bond the sheets, obtaining MXenes sheets from MAX requires strong chemicals to break the bonds to obtain thin layers.

Ti_3C_2 is one of the most used MXenes. It was synthesized for the first time by Barsoum and Gogotsi group (Naguib et al. 2011) and obtained by reaction of hydrofluoric acid HF on Ti_3AlC_2. This reaction breaks the bond that connects Al to two MX sheets and replaces the Al atoms with hydroxyl groups. With only hydrogen bonds holding the sheets together, exfoliation can be done simply by

sonication, producing Ti_3C_2Tx sheets, with T representing surface OH groups (Figure 1.24).

Subsequently, a whole series of MXenes were synthesized and are described in several review articles (Naguib et al. 2012, 2014; VahidMohammadi et al. 2021; Alwarappan et al. 2022; Chen et al. 2023). The properties of these nanomaterials (high conductivity, high chemical stability, ease of implementation, biocompatibility and ability to produce large quantities) make them particularly attractive for many applications (catalysis, batteries, supercapacitors, electromagnetic shielding, medical treatments and detection devices). Although often compared to graphene because of their high conductivity, with properties that depend on their surface Tx terminations, their use for detecting various analytes is only envisaged in certain composites. This generates heterojunctions, which increase chemical interactions with the analyte and induce strong variations in conductivity.

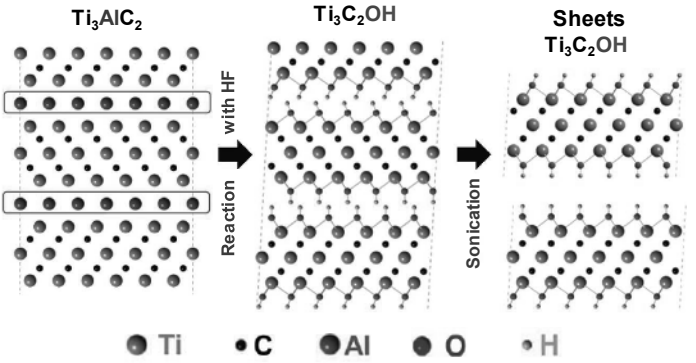

Figure 1.24. *Principle of the method of obtaining Ti_3C_2OH sheets from Ti_3AlC_2. Reacting it with HF replaces the Al atoms, which bond the Ti_3C_2 sheets with weakly binding OH groups, facilitating the exfoliation process by sonication. Adapted from Naguib et al. (2011). For a color version of this figure, see www.iste.co.uk/lacaze/nanotechnologies.zip*

1.2.4.3. *Phosphorene*

Phosphorene is a p-type semiconductor (Cho et al. 2016) with one or more BP monolayers. It was first isolated in 2014 by the mechanical exfoliation of BP, using the scotch tape method developed by Geim and Novoselov to extract graphene from graphite. Subsequently, chemical exfoliation methods of BP in the liquid phase, liquid phase exfoliation (LPE), were proposed using various organic solvents, mainly N-methyl pyrrolidone (NMP), dimethylformamide (DMF), as well as aqueous media with added surfactants. These were each subjected to vigorous

sonication. A good description of these preparation techniques can be found in recent papers (Gusmao et al. 2017; Yang et al. 2018).

One of the unusual characteristics of phosphorene is that its band gap varies between 0.3 and 2.2 eV when it passes from a compact solid state (BP) to the final single layer state (Figure 1.25).

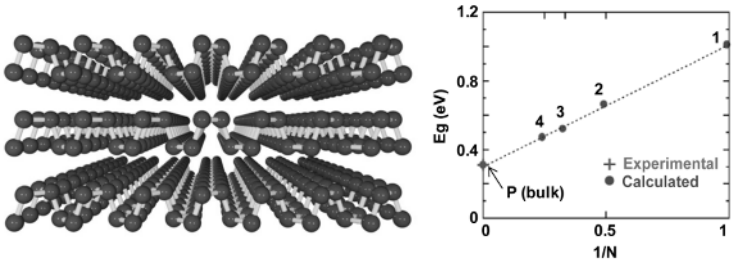

Figure 1.25. *Structural and energetic characteristics of phosphorene. (a) Perspective view of phosphorene sheets. (b) Variation in band gap as a function of the number N of layers (4, 3, 2 and 1). Adapted from Liu et al. (2014a). For a color version of this figure, see www.iste.co.uk/lacaze/nanotechnologies.zip*

Phosphorene is characterized by a high hole mobility, between 600 and 1,000 $cm^2 V^{-1} s^{-1}$, and, when incorporated in an FET structure, the "On/Off" ratio of the drain current is also high, around 10^3–10^5 (Liu et al. 2014a). These properties make phosphorene an intermediate material between graphene and TMDs, well suited to produce chemical sensors. However, its sensitivity to air humidity requires extra precautions during use and protection of the sensitive layer. Dispersing gold or platinum NPs onto the surface of phosphorene modifies its electronic properties, making it comparable to an n-type SC with very good stability over several months (Cho et al. 2017). Recently, the pulsed laser of a fine BP powder suspended in NMP produced phosphorene with greater stability when the BP precursor is obtained by the high energy mechanical milling (HEMM) of red phosphorus (the most stable form of phosphorus) (Zhang et al 2019a). Other methods including exfoliation by anodic electrolysis of BP in a saline environment (0.5 M Na_2SO_4) have also been proposed and give stable phosphorene nanosheets.

1.2.5. *Metal organic frameworks (MOFs)*

MOFs are formed directly by self-assembly reactions between metal ions or metal clusters and organic compounds, with reactive functions in determined

directions (multitopic ligands). Like porous crystals, they have the advantage over other porous inorganic materials (zeolites, silicas, etc.) in that it is possible to modulate porosity and "host–guest" interactions by the choice of reagent used in the synthesis process. The interest in MOFs has continued to grow since their discovery, giving rise to many applications which range from the enhanced recovery of hydrocarbons to the capture of gases or their separation, as well as their use in the design of sensors and specific capillary electrophoresis devices (see Chapter 2). Compounds similar to MOFs, but entirely organic, have also been developed and differ from MOFs in that their bonds are covalent, hence their name covalent organic frameworks (COFs) (Geng et al. 2020).

1.2.6. *Methods for manufacturing MOFs*

MOFs are obtained according to two main methods. The first involves a crosslinking reaction between predefined inorganic blocks and organic ligands, which leads to hybrid crystal structures with controlled porosities. The second uses an existing MOF and transforms it through ligand substitution to obtain new functionalities.

Directly obtaining MOFs using this crosslinking method was developed on a large scale by Yaghi (USA) and Férey (France) and their teams. The synthesis of hybrid, crystalline and robust materials with controlled and predefined porosities is described in several review articles (Yaghi et al. 2003; Férey 2008). This method generates an MOF result from the self-assembly between preconstructed inorganic blocks, known as secondary building units (SBU), and rigid and directional organic ligands.

Remarkably, SBU blocks retain their entire geometric structure during the crosslinking reaction. The wide range of rigid organic compounds and inorganic SBUs available makes it possible to obtain an infinite number of materials whose porosity can be determined in advance.

These synthesis principles are described by Yaghi et al. (Li et al. 1999) for one of the very first examples of MOF production (MOF-5) where zincates arranged in the form of a super-tetrahedron-like cluster (SBU) react with rigid organic ligands, such as 1,4-benzene dicarboxylate (BDC) (Figure 1.26).

Crosslinking takes place in a hot organic medium in a closed reactor. An MOF cubic network, where the four zincates are linked together by a common oxygen (O) and six carboxylate ligands ($-CO_2$) coming from the six BDCs, gives the stoichiometry $Zn_4(O)(BDC)_3$.

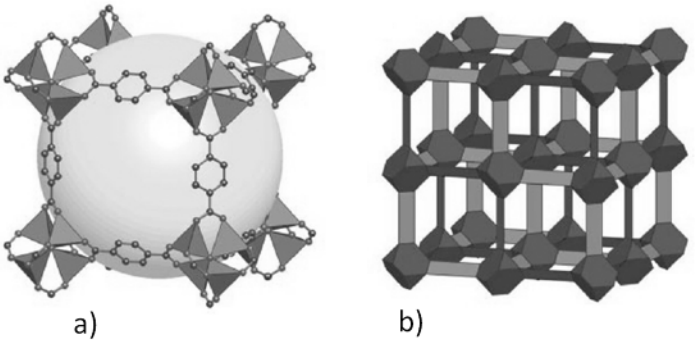

Figure 1.26. *Structure and topology of MOF-5. (a) Representation of the unit cell obtained by reaction between the zincates (blue tetrahedra) and the carboxylate groups of the BDCs (the oxygen atoms are in red, the carbons in black). The yellow sphere represents the maximum occupancy volume of the internal cavity defined by eight groups of four zincates and twelve BDCs (diameter of the occupancy sphere ~1.2 nm). (b) Representation of the cubic network of MOF-5. Assemblies formed by four zincates (SBU) are represented in red by truncated tetrahedra; the links between zincates correspond to the BDCs and are represented in blue. Adapted from Yaghi et al. (2003). For a color version of this figure, see www.iste.co.uk/lacaze/nanotechnologies.zip*

These porosity properties can be further enhanced by choosing larger organic ligands, while retaining the topology of the crystal (isocrosslinking principle). A few years later, Yaghi et al. synthesized a series of MOFs, producing porous systems whose cavities have pores that can be predetermined by the choice of the ligands binding the inorganic SBUs. Thus, by using the same inorganic cluster formed by the four ZnO_4 derivatives (identical to that of MOF-5) and by choosing linear, rigid organic ligands of increasingly longer lengths, ranging from fumarate to TPDC (terphenyl- 4,4'-dicarboxylate), the pore size is then considerably enlarged. Its volume is 7.8 times greater than for MOFs obtained with fumarate (Figure 1.27)[26]. Intermediate sizes are obtained with ligands like BDC (phenyl-1,4-dicarboxylate and MOF-5) and BPDC (biphenyl-4,4′-dicarboxylate and IRMOF-10).

26 Compared to the various usual microporous materials such as zeolites (alumino silicates AlO_4^{5-} and SiO_4^{4-}), silicas (SiO_2) or active carbons for which the gas adsorptions measured by the Brunauer–Emmett–Teller (BET) method are between 900 and 1200 m^2/g, and their porosity volumes are, respectively, 0.3 g/cm^3, 1.15 g/cm^3 and 0.60 g/cm^3, MOFs have significantly higher gas absorption possibilities ranging from more than 2,000 m^2/g with MOF-5 to values over 7,000 m^2/g with NU-110, with very low mass densities (Furukawa et al. 2013). The BET method is used to determine the equivalent surface area of a porous material from the quantity of nitrogen adsorbed in the pores of the material at 77 K.

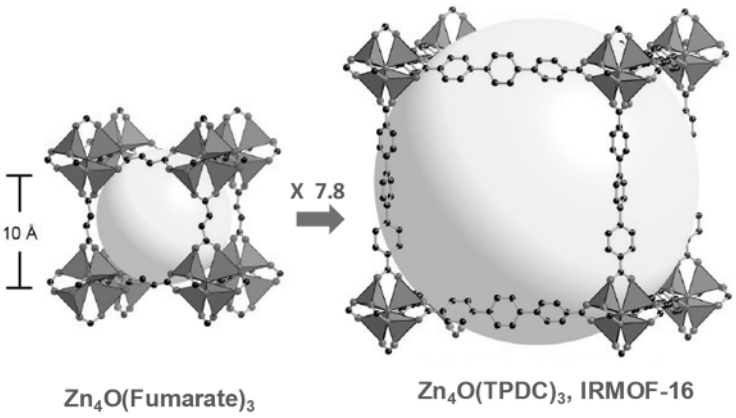

Figure 1.27. *Principle of synthesis by isoreticulation. The use of fumarate then terphenyl-4,4''-dicarboxylate (TPDC) increases the bond lengths between the SBUs (ZnO_4) while retaining the initial topology and increasing the size of the pore in the MOF cubic network. As with the previous figure, the yellow sphere represents the maximum size of a chemical species that can be inserted into the cavity. Adapted from Furukawa et al. (2013). For a color version of this figure, see www.iste.co.uk/lacaze/nanotechnologies.zip*

More than 20,000 MOFs have been synthesized over the last 10 years by changing the nature of both the ligands and the inorganic SBUs, whose varying structures give very varied application possibilities. Records have been set for BET adsorption measurements reaching more than 7,000 m^2/g, with predictable theoretical values of more than 10,000 m^2/g, (Farha et al. 2012). Finally, it is important to point out that these MOFs can be used to synthesize nano-MOFs (n-MOFs) in a micellar constrained medium, which introduces the possibility of luminescent n-MOFs, and again, potential application in the field of biomedical imaging (Carne et al. 2011).

Another layer-by-layer synthesis technique was also used to manufacture MOF films adsorbed onto a solid support (Ohnsorg et al. 2015), by functionalizing the substrate with long hydrocarbon chain molecules, capable of surface self-assembly. Their reactive end (such as –COOH) can bind with the ligand and induce the growth of an MOF film and thus obtain a surMOF attached to the substrate. For example, a surMOF film with the global formula $Cu_3(TMA)_2$, known as HKUST-1[27], is often used in the design of optoelectronic devices in thin layers. It is obtained after a series

27 Most MOFs are identified by acronyms that describe the original laboratory or university where they were discovered and produced. HKUST is the acronym for Hong Kong University of Science and Technology.

of immersion cycles, rinsing and drying a gold surface functionalized by a self-organized layer of 16-mercaptohexadecanoic acid[28]. This technique is very interesting because it allows an MOF film of controlled thickness and dimensions to be locally attached onto a suitably functionalized surface. We can thus design various detection devices based on optical or electronic responses. Adding their modular porosity, these devices are suitable for the selective absorption of gases and molecules (Falcaro et al. 2014).

By playing on both the nature of the ligands and that of the SBUs, many structures have been manufactured, giving them varied applications in fields such as medical imaging, drug vectorization (Horcajada et al. 2010), catalysis, the creation of optoelectronic devices, or the improvement of proton conduction in H_2/O_2 fuel cells. The storage of gases and their separation, the identification of molecules and the functionalization of MOFs to create multiple luminescence centers are other application areas. Together an adjustable porosity and luminescence, obtained according to the choice of ligands and metal clusters, make extremely well-suited MOFs for the development of photoluminescent devices used in the detection of chemical species. They are also involved in the formation of electrophoresis columns where porosity plays a determining role (see Chapter 2).

The luminescence of an MOF can have very different origins: it can be due to the ligand, the metal, the insertion of fluorescent species into the MOF or even antenna effects between the metal and the ligand corresponding to energy transfers. These luminescence properties can be used in a variety of ways. When the ligand and the metal are fluorescent, we can use the MOF porosity to insert a particular chemical species. If this species quenches the fluorescence of the ligand or the metal (quenching effect), then the MOF can be used to detect the species in question. This property can be used to detect explosives (Allendorf et al. 2009; Lan et al. 2009; Hu et al. 2014b).

In summary, synthesized by assembling metal ions with organic ligands, MOFs are a new class of crystalline and hybrid three-dimensional porous materials, distinguished from traditional porous materials (zeolites, activated carbons, porous silicas, etc.) by their modular porosity and by the possible introduction of various functionalities into their pores. This makes them suitable for a wide range of applications. Their relatively simple manufacture, which does not require very high temperatures (condensation generally takes place in an organic medium and for

28 The first cycle involves first immersing it in a copper acetate solution, then, after rinsing and drying, immersing it in a 1,3,5-benzene tricarboxylic acid solution (trimesic acid [TMA]), which leads to the first surMOF layer of approximately 2 nm thick when the reactions are carried out at 25°C. This production cycle can be repeated several times and the thickness of the film increases linearly with the number of cycles (Ohnsorg et al. 2015).

temperatures between 100 and 200°C), makes them more accessible than many comparable materials. Among their numerous applications, three applications are now proving extremely important: the separation and storage of gases, proton conduction with a potential application to hydrogen fuel cells and applications linked to the detection of chemical species due to optical properties of fluorescence and controlled porosity.

1.3. Conclusions

The last 20 years have seen the emergence of new families of carbon nanomaterials that have established themselves through their properties and the new solutions they provide in energy, electronics, biology and sensors.

Fullerenes, CNTs, graphene and their derivatives have become essential materials despite having a simple structure based solely on sp^2 hybridized carbon chains. Their properties differ depending on their dimensional characteristics, 0D for fullerenes, 1D for CNTs and 2D for graphene. CNTs, graphene and their functionalized derivatives have been particularly successful because of their exceptional electrical and mechanical properties, which have given rise to new plastic hybrid materials with improved mechanical and electrical properties and to the production of composite electrodes used in electrocatalysis, energy storage and conversion, and analysis.

Graphene and its derivatives (GO) are undoubtedly the compounds with the greatest number of applications and the greatest development with the manufacture of plasticized ribbons, foams, papers, or even fibers, bringing together both excellent electrical and mechanical properties. Nanometric graphene fragments are a new variety comparable to QDs (GQDs), characterized by their fluorescence properties and by non-zero forbidden energy bands, which make them suitable for the construction of various optoelectronic devices.

NDs, carbon nanoparticles in the form of CQDs, are a new family of materials; they are distinguished by their small size, less than 10 nm, and by different types of carbon–carbon bonds involving, in variable proportions, hybridized sp^2 and sp^3 carbons. For NDs, these are mainly bonds between sp^3 carbons, while for CQDs, the particle nucleus is essentially composed of graphitic sp^2 carbons. These are also commercialized materials, much easier to obtain than CNTs, fullerenes and graphene, and therefore accessible at lower costs. For certain electrochemical applications (energy storage, production of electrolytic capacities), CQDs compete with activated carbon. Their use is also linked to their fluorescence properties, differentiating them from intrinsically non-luminescent fullerenes, CNTs and graphene. Furthermore, the presence of hydrophilic functional groups on the surface

makes them soluble in an aqueous medium, and due to their non-toxicity, they are considered excellent candidates for medical imaging.

In the case of inorganic nanomaterials, three main families can be distinguished: metallic nanoparticles (MNPs), semiconductor nanoparticles or QDs, and, more recently, two-dimensional nanomaterials formed from transition metal chalcogenides (TMDs). This last category also includes Mxenes and phosphorene, which are promising in various applications ranging from drug delivery to energy storage. The most common applications relate to electronic devices (especially transistors), optoelectronic devices and gas sensors.

Metallic gold NPs (AuNPs) are the most widely studied and have given rise to many analytical applications. Their optical properties, however, differ considerably depending on their size. For sizes less than 3 nm, their light absorption is like that of a molecular compound, while for larger sizes, the metallic character becomes predominant and their absorption is plasmonic. We observe luminescence properties for very small NPs (NCs), whose intensities depend on the NP functionalization mode. As with carbon nanomaterials, and due to their lack of toxicity, these gold NCs are used essentially for their fluorescence properties in biomedical imaging applications and the detection of compounds in very low concentrations. On the contrary, larger gold NPs are mainly used for their quenching properties and ability to enhance numerous spectroscopies.

Semiconductor QDs, also wet synthesized, are another family of nanomaterials, particularly sought after for their exceptional fluorescence properties, far superior to organic fluorophores. In the core/shell form (CdSe/ZnS type), the photofluorescence quantum yields are close to one, their photostability is very good and without intermittency, and very pure fluorescence colors are obtained depending on the composition and the size of the QDs. These PL properties are preserved in electroluminescent devices and mean that QDs are now considered among the most efficient nanomaterials to produce color screens and for the more general design of optoelectronic devices, also applicable in analytical chemistry.

The abundant and easily synthesized two-dimensional nanosheets of TMDs, including MoS2 and WS2, are currently 2D nanomaterials of growing interest. Their enthusiasm is comparable to that experienced by graphene when it was discovered. Their semi-conduction and intercalation properties make them materials of choice for applications ranging from plastic electronics to energy storage. They also lend themselves easily to the production of various optoelectronic systems. They are therefore used to produce various sensors for detecting gases and pollutants in trace amounts.

Of the hybrid and composite materials, three-dimensional organometallic networks (MOFs) are also an essential family of nanoporous compounds, which can be synthesized with a moderate energy cost compared to zeolites. The architecture of these compounds can be modulated infinitely, which makes it possible to define the dimensions of the pores and the crystallographic characteristics in advance and, thus, to best optimize the structure for a specific function in gas separation or analytical chemistry.